Marcks and Marcks-like 1 proteins promote spinal cord development and regeneration in *Xenopus*

Mohamed El Amri[1,2], Abhay Pandit[2], Gerhard Schlosser[1]*

[1]School of Biological and Chemical Sciences, University of Galway, Biomedical Sciences Building, Newcastle Road, Galway H91 W2TY, Ireland

[2]SFI Research Centre for Medical Devices (CÚRAM), University of Galway, Biomedical Sciences Building, Newcastle Road, Galway H91 W2TY, Ireland

***Corresponding author**:
School of Biological and Chemical Sciences, University of Galway, Biomedical Sciences Building, Newcastle Road, Galway H91 W2TY, Ireland, Phone: 00353-91-495978, E-mail: gerhard.schlosser@universityofgalway.ie

Abstract

Marcks and Marcksl1 are abundant proteins that shuttle between the cytoplasm and membrane to modulate multiple cellular processes, including cytoskeletal dynamics, proliferation, and secretion. Here, we performed loss- and gain-of-function experiments in *Xenopus laevis* to reveal the novel roles of these proteins in spinal cord development and regeneration. We show that Marcks and Marcksl1 have partly redundant functions and are required for normal neurite outgrowth and proliferation of neuro-glial progenitors during embryonic spinal cord development and for its regeneration during tadpole stages. Rescue experiments in Marcks and Marcksl1 knockout animals further suggested that some of the functions of Marcks and Marcksl1 in the spinal cord are mediated by phospholipase D (PLD) signaling. Taken together, these findings identify Marcks and Marcksl1 as critical new players in spinal cord development and regeneration and suggest new pathways to be targeted for therapeutic stimulation of spinal cord regeneration in human patients.

Introduction

Spinal cord injury in humans is a life-changing condition with no effective treatment. However, many non-mammalian vertebrates can fully regenerate their spinal cords after injury (Lee-Liu, Edwards-Faret, Tapia, & Larrain, 2013, Alunni & Bally-Cuif, 2016, Rodemer, Hu, Selzer, & Shifman, 2020). In the clawed toad *Xenopus*, tadpoles can fully regenerate the spinal cord; however, this capacity is lost during metamorphosis (Beattie, Bresnahan, & Lopate, 1990, Gibbs, Chittur, & Szaro, 2011). Therefore, *Xenopus* offers a rare opportunity to compare cellular and molecular responses to spinal cord injury (SCI) in a regeneration-competent system with a regeneration-incompetent system in the same species. Thus, differences between the responses to SCI in the two stages likely have some functional implications for the difference in regenerative capacity rather than reflecting other phylogenetically accumulated differences in development, as may be the case when different species are compared.

A recent proteomic screen to identify proteins differentially regulated in regeneration-competent tadpoles versus regeneration-incompetent froglets after SCI identified Marcks and Marcksl1 as proteins that are highly upregulated at the tadpole stage but downregulated in froglets (Kshirsagar, 2020), suggesting a potential role for these proteins in spinal cord regeneration.

Marcks is an abundant and widely expressed protein with three highly conserved functional domains: an effector domain (ED), a Marcks Homology 2 (MH2) domain, and a myristoylation domain (Brudvig & Weimer, 2015, El Amri, Fitzgerald, & Schlosser, 2018). Marcks-like protein 1 (Marcksl1) shares strong homology and functionality with Marcks (Stumpo et al., 1998). In an unphosphorylated state, the positively charged ED of Marcks attaches to the plasma membrane, and the myristoylation site tethers the protein to the membrane (Kim, Blackshear, Johnson, & McLaughlin, 1994, McLaughlin & Aderem, 1995). However, when the ED is phosphorylated by Protein kinase C (PKC), thereby acquiring more negative charges, Marcks translocates to the cytoplasm (Brudvig & Weimer, 2015; McLaughlin & Aderem, 1995).

Depending on their phosphorylation status and subcellular localization, Marcks and Marcksl1 regulate multiple processes in the cell. For example, they have been shown to modulate the polymerization and cross-linking of actin filaments, recruit secretory vesicles to the embrane, and interact with phosphatidylinositol 4,5-bisphosphate (PIP_2), thereby regulating multiple signaling pathways downstream of PIP_2 such as phospholipase C (PLC) and phospholipase D (PLD) dependent pathways (Hartwig et al., 1992, Morash, Rose, Byers,

Ridgway, & Cook, 1998, Yarmola, Edison, Lenox, & Bubb, 2001, Wohnsland, Schmitz, Steinmetz, Aebi, & Vergeres, 2000, McLaughlin, Wang, Gambhir, & Murray, 2002, Sundaram, Cook, & Byers, 2004, Xu et al., 2014). Consequently, Marcks and Marcksl1 affect cytoskeletal dynamics, cell migration, secretion, cell proliferation, and differentiation in the nervous system and other tissues (Brudvig & Weimer, 2015, El Amri et al., 2018).

Importantly, Marcks and Marcksl1 proteins were found to be upregulated in several different regenerative processes, such as lens regeneration in newts, fin regeneration in lungfish and bichirs, tail regeneration in lizards, and cardiac tissue regeneration following infarction in mice (Bock-Marquette et al., 2009, Sousounis et al., 2014, Nogueira et al., 2016, Alibardi, 2017, Lu et al., 2019). Moreover, a Marcks- and Marcksl1-like protein in axolotls (AxMLP) initiates an early proliferative response in axolotl tail and limb regeneration (Sugiura, Wang, Barsacchi, Simon, & Tanaka, 2016). In the nervous system, Marcks and Marcksl1 are also significantly upregulated in outgrowing and/or regenerating neurites of facial motor neurons, dorsal root and superior cervical ganglia, in the optic nerve and during axonal sprouting after brain stroke, suggesting an essential role for Marcks and Marcksl1 in neurite outgrowth and regeneration in both the peripheral and central nervous systems (McNamara, Jiang, Streit, & Lenox, 2000, Carmichael et al., 2005, Szpara et al., 2007, Veldman, Bemben, Thompson, & Goldman, 2007).

In this study, we combined Marcks and Marcksl1 gain- and loss-of-function experiments in *Xenopus laevis* with histological and behavioral analyses to show, for the first time, that Marcks and Marcksl1 also play essential roles during spinal cord development and regeneration. We demonstrate that both proteins have partly redundant functions and are required for normal neurite outgrowth and the proliferation of neuro-glial progenitors during the development of the spinal cord, as well as for its regeneration after full transection. Rescue experiments with pharmacological compounds in Marcks and Marcksl1 knockout animals further suggest that at least some of the functions of Marcks and Marcksl1 in the spinal cord are mediated by PLD signaling. Taken together, these findings identify Marcks and Marcksl1 as critical new players in spinal cord development and regeneration and highlight the power of *Xenopus* as an experimental model for identifying new pathways required for regeneration competence.

Results

Marcks and Marcksl1 are expressed in the developing Xenopus spinal cord

To elucidate the role of Marcks and Marcksl1 for spinal cord development, we first analyzed mRNA expression of *marcks.S*, *marcksl1.S,* and *marcksl1.L* in embryos of *Xenopus laevis* at stages 26 and 34 (early and late tailbud stage, respectively). Due to the 94% sequence identity between *marcks.S* and *marcks.L* mRNAs, the *marcks.S* probe is expected to cross-react with *marcks.L,* while *marcksl1.S* and *marcksl1.L* mRNA have only 84% identity and show slightly different expression suggesting that they exhibit only limited if any cross-reactivity. Whole-mount in situ hybridization showed that all of these genes have a similar pattern of expression (Fig. 1 A-G, Fig. S1). They are strongly expressed in the brain and spinal cord as well as in the pharyngeal arches, somites, intermediate mesoderm, and blood islands of the ventrolateral mesoderm. *marcks*.S is more broadly distributed through the entire brain, whereas *marcksl1.L* and *marcksl1.S* have a more restricted expression and are absent from the forebrain. Vibratome sections of stage 34 embryos after whole-mount in situ hybridization confirmed the expression of all genes throughout the spinal cord as well as in the brain, lens, pharyngeal arches, somites, and other mesodermal derivatives (Fig. 1 H, I; Fig. S2-4). They also reveal the expression of all genes in the epidermis and of *marcks.S* in the otic vesicle and show that *marcksl1.S* has a weaker and more restricted expression in the brain and spinal cord than *marcksl1.L*.

We next used two polyclonal antibodies raised against epitopes shared between *Xenopus laevis* Marcks.S and Marcks.L protein and between Marcksl1.S and Marcksl1.L, respectively, to clarify the subcellular distribution of Marcks and Marcksl1 proteins in the developing spinal cord. These antibodies specifically recognize Marcks and Marcksl1 proteins, respectively, without cross-reactivity (Fig. S5). Confocal microscopy of embryos injected with mRNAs encoding a membrane-tethered form of GFP (*memGFP*) and transversely sectioned at stage 26 revealed that Marcks and Marcksl1 are mostly associated with outer cell membranes. This is true for the ventricular zone, where progenitor cells are located, and the adjacent mantle zone, which harbors migrating and differentiating neurons (Fig. 1 K-P). In addition, a subset of cells in both ventricular and mantle zones shows cytoplasmic expression of Marcks and Marcksl1. Marcks, but not Marcksl1 was also occasionally seen in cell nuclei.

Because shuttling between the membrane and cytoplasm is essential for the function of Marcks and Marcksl1 in other developmental contexts (El Amri et al., 2018), their subcellular localization to membranes and cytoplasm in the spinal cord and their widespread distribution in the developing spinal cord suggests that these proteins may play hitherto unrecognized roles during normal spinal cord development. To test this hypothesis, we next used two independent approaches, injection of antisense Morpholino oligonucleotides (MO) and CRISPR/Cas9-mediated gene editing, to determine how knockdown/-out of these proteins affects neurite

outgrowth, cell proliferation, and neuro-glial progenitor populations during spinal cord development.

Marcks and Marcksl1 are required for normal neurite outgrowth during spinal cord development

We first studied the role of Marcks and Marcksl1 in neurite outgrowth in the spinal cord individually by injecting a single blastomere in 4-to-8-cell stage embryos with either an MO blocking the translation of both *marcks.L* and *marcks.S* or with a mixture of two MOs blocking the translation of *marcksl1.L* and *marcksl1.S,* respectively. This resulted in the unilateral knockdown of the respective proteins on the injected side of the embryo, whereas the uninjected side developed normally. *myc-GFP* mRNA was co-injected to identify the injected side. The effectiveness and specificity of all MOs used were validated by in vitro transcription and translation of the various proteins in the presence or absence of the appropriate MO (Fig. S6). None of these injections led to significant alterations in immunostaining for the neurite marker acetylated tubulin on the injected side of the spinal cord relative to the uninjected side in stage 34 embryos compared to an unspecific control MO (Fig. 2 A-C). However, when the three MOs targeting *marcks.S/L*, *marcksl1.S,* and *marcksl1.L* were co-injected, thus blocking all four homeologs (4M MO), acetylated tubulin staining was significantly decreased on the injected side (Fig. 2, D, E, G). Co-injection of mRNA constructs encoding chicken Marcks and *Xenopus tropicalis* Marcksl1, which were selectively mutated to prevent MO binding, resulted in complete rescue of acetylated tubulin staining, confirming the specific action of the MOs used (Fig. 2 F, G). This suggests that Marcks and Marcksl1 are required for neurite outgrowth during spinal cord development but act in a largely redundant fashion. To account for these overlapping functions, we aimed to simultaneously knockdown or knockout all four proteins (Marcks.L/S, Marcksl1.L/S) for the rest of our study.

To verify the results of our MO knockdown experiments, we analyzed F0 embryos after CRISPR-Cas9 gene editing. For these experiments, single-guide RNA constructs targeting *marcks.S, marcks.L*, *marcksl1.S,* and *marcksl1.L* genes were co-injected with Cas9 as a ribonucleoprotein (RNP) and *myc-GFP* mRNA into one blastomere during the 1-cell stage for genotyping or the 4-to-8 cell stage for phenotypic analysis. At later embryonic stages (stage 26-42), genomic DNA was extracted from some of the embryos, sequenced, and analyzed with Synthego Inference for CRISPR Edits (ICE) to determine the frequency with which indels were generated in the targeted region (indel score) as well as the frequency of indels with frameshifts

176 (knockout score). Sibling embryos were used for phenotypic analysis. In control experiments,
177 we either injected Cas9 protein and *myc-GFP* mRNA alone or injected a sgRNA targeting
178 *slc45a2* (DeLay et al., 2018), encoding a protein that mediates melanin synthesis, Cas9
179 proteins, and *myc-GFP* mRNA. When analyzing CRISPR/Cas9 edited animals in the F0
180 generation, a considerable and variable extent of mosaicism has to be taken into account
181 because different gene editing events may occur in different subsets of cells (Blitz, Biesinger,
182 Xie, & Cho, 2013; DeLay et al., 2018). We, therefore, first tested a range of different sgRNAs
183 to ensure high overall gene editing and knockout efficiencies.

184 We first validated our CRISPR knockout procedure using the control gene *slc45a2*.
185 Embryos injected during the 1-cell stage with *slc45a2* RNPs and analyzed at stages 37-46 lost
186 pigmentation in both eyes, whereas embryos injected during the 2-to-4-cell stage showed loss
187 of pigmentation only in the injected side. Confirming a previous report (DeLay et al., 2018),
188 genomic sequencing revealed a high indel score (93%) and knockout score (67-68%) in these
189 embryos (Fig. S7). Almost all surviving embryos displayed visible oculocutaneous albinism,
190 with the majority showing almost no eye pigment (Fig. S7).

191 Next, we designed, synthesized, and tested a total of 18 sgRNA transcripts targeting either
192 *marcks.L/S* or *marcksl1.L/S* (sgRNAs were designed to target both homeologs of each gene)
193 and selected the sgRNA transcripts creating the highest and most consistent number of indels
194 and knockout scores for each pair of genes - named *marcks.L/S* and *marcksl1.L/S* sgRNA,
195 respectively - for further experiments (Figs. S8-11). The *marcks.L/S* sgRNA introduced indels
196 in 88% of the targeted DNA from *marcks.L* exon 1 (8 embryos) and 84% from *marcks.S* exon
197 1 (8 embryos), with an average of 78% and 76%, respectively, consisting of frameshift
198 mutations which may contribute to a functional knockout (Figs. S8 C, S9 C). The *marcksl1.L/S*
199 sgRNA introduced indels in 73% of the targeted DNA from *marcksl1.L* exon 2 (6 embryos)
200 and 73% from *marcksl1.S* exon 2 (7 embryos), with an average of 50% and 47%, respectively,
201 being out-of-frame (Figs. S10 C, S11 C). We also confirmed by immunohistochemistry that
202 co-injection of *marcks.L/S* and *marcksl1.L/S* sgRNA, which is predicted to edit all four
203 homeologs (henceforth denoted as 4M CRISPR) drastically reduced immunostaining for
204 Marcks and Marcksl1 protein on the injected side (Fig. S6 B-G), indicating that protein levels
205 are reduced in gene-edited embryos.

206 Similar to the knockdown of the proteins by MOs, the unilateral CRISPR-mediated
207 knockout of all Marcks and Marcksl1 homeologs (4M CRISPR) led to a significant reduction
208 in acetylated tubulin staining on the injected side compared to Cas9 and *slc45a2* controls (Fig.
209 2 H-K). Conversely, overexpression of both proteins by injection of *marcks* and *marcksl1*

210 mRNA at two different doses (100 or 300 pg each) together with *myc-GFP* mRNA resulted in
211 a significant increase in acetylated tubulin staining on the injected side compared to that in
212 control embryos injected with *myc-GFP* mRNA alone (Fig. S12). Taken together; these results
213 suggest that Marcks and Marcksl1 play essential roles for neurite outgrowth during normal
214 embryonic development of the *Xenopus* spinal cord, with elevated levels of Marcks and
215 Marcksl1 being able to further promote neurite outgrowth.
216

217 ***Marcks and Marcksl1 are required for the proliferation of neuro-glial progenitors during***
218 ***spinal cord development***

219 Next, we tested whether Marcks and Marcksl1 are required for the proliferation of neuro-
220 glial progenitor cells during spinal cord development. After unilateral injection with a cocktail
221 of the three MOs targeting *marcks.S/L*, *marcksl1.S* and *marcksl1.L* (4M MO) or with the
222 combined *marcks.L/S* and *marcksl1.L/S* sgRNAs (4M CRISPR), we analyzed the number of
223 cells in mitosis in the spinal cord of stage 34 embryos by immunostaining against phospho-
224 histone H-3 (PH3). In both control and experimental animals, PH3-positive nuclei are confined
225 to the ventricular zone at this stage, where neuro-glial progenitors reside (Fig. 3 A-C, E-G).
226 The proportion of PH3-positive ventricular nuclei on the injected side (expressed as the ratio
227 between injected/uninjected sides) was significantly reduced in both experiments compared to
228 control injections (Fig. 3 A-H). Conversely, the injection of *marcks* and *marcksl1* mRNA
229 together with *myc-GFP* mRNA resulted in a significant increase in the proportion of PH3-
230 positive ventricular nuclei on the injected side compared to control embryos injected with *myc-*
231 *GFP* mRNA alone (Fig. S13). These observations indicate that Marcks and Marcksl1 are
232 required for normal patterns of cell proliferation in the ventricular zone of the developing spinal
233 cord. In addition, increased levels of Marcks and Marcksl1 are sufficient to further promote
234 cell proliferation.
235 To directly test the role of Marcks and Marcksl1 for neuro-glial progenitors, we next
236 immunostained spinal cords of stage 34 embryos for the progenitor markers Sox2 or Sox3 after
237 unilateral injection of *marcks.L/S* and *marcksl1.L/S* sgRNAs. The numbers of Sox2- or Sox3-
238 positive nuclei on the injected side (expressed as a ratio between injected/uninjected sides) was
239 significantly reduced as compared to control embryos injected with *slc45a2* sgRNAs or with
240 Cas9 alone (Fig. 3 I-M). This indicates that Marcks and Marcksl1 are required for maintaining
241 a normal pool of neuro-glial progenitor cells during spinal cord development. This may at least
242 partly result from the role of both proteins in promoting the proliferation of these neuro-glial

243 progenitors, as described above, but additional roles for the survival and maintenance of neuro-
244 glial progenitors cannot be ruled out.
245
246 ***PLD and other signaling pathways mediate the functions of Marcks and Marcksl1 during***
247 ***spinal cord development***

248 Since Marcks and Marcksl1 are known to be multifunctional proteins, we next asked which
249 signaling pathways may mediate the effects of Marcks and Marcksl1 during spinal cord
250 development. Our experiments described so far suggested essential functions of these proteins
251 in both proliferation control and neurite outgrowth. We, therefore, focused on the
252 phospholipase D (PLD) dependent signaling pathway since previous studies have suggested
253 that PLD signaling is activated downstream of Marcks (Morash, Byers, & Cook, 2000; Morash
254 et al., 1998) and has essential functions in both the regulation of mitosis and of cytoskeletal
255 dynamics including neurite outgrowth (Kam & Exton, 2001, Foster & Xu, 2003, Zhang et al.,
256 2004, Brown, Thomas, & Lindsley, 2017). To activate and inhibit PLD signaling, we used
257 Sphingosine-1-phosphate (S1P) and 5-Fluoro-2-indolyl des-chlorohalopemide (FIPI),
258 dissolved in 2% DMSO, respectively (Meacci et al., 2003, Monovich et al., 2007, Su et al.,
259 2009).
260 Embryos were unilaterally injected with *marcks.L/S* and *marcksl1.L/S* sgRNAs (4M
261 CRISPR), as described above, were then raised for one day before fixation in PLD activators
262 or inhibitors and were analyzed at stage 34 by immunostaining for the neurite marker acetylated
263 tubulin and the mitosis marker PH3. 4M CRISPR-injected control embryos were raised in 2%
264 DMSO and similarly analyzed. Compared to DMSO-treated controls, incubation in the PLD
265 activator S1P significantly increased the intensity of acetylated tubulin staining (Fig. 4 A) as
266 well as the proportion of PH3-positive cells (Fig. 4 B) on the CRISPR-injected side relative to
267 the uninjected side, whereas the PLD inhibitor FIPI had no significant effect (Fig. 4 A, B). The
268 ability of PLD activation but not inhibition to rescue the deficiencies in the CRISPR-injected
269 embryos suggests that Marcks and Marcksl1 promote neurite outgrowth and progenitor
270 proliferation at least partly by a PLD-dependent mechanism.
271 Because PLD signaling downstream of Marcks has previously been suggested to be PIP_2
272 dependent (Morash et al., 2000; Sundaram et al., 2004), we next tested whether enhancement
273 or inhibition of PIP_2 synthesis is also able to modulate the effects on spinal cord development
274 in our CRISPR-injected embryos. For PIP_2 biosynthesis enhancement and inhibition, we
275 incubated 4M CRISPR-injected embryos in N-Methyllidocaine iodide (NMI) and ISA-2011B,

respectively (Lee, Tardi, Man, & Choy, 1995, Semenas et al., 2014). Compared to DMSO-treated controls, embryos in which NMI enhanced PIP_2 biosynthesis showed a significant increase in the intensity of acetylated tubulin staining (Fig. 4 C) as well as in the proportion of PH3-positive cells (Fig. 4 D) on the CRISPR-injected side relative to the uninjected side. In contrast, the PIP_2 synthesis inhibitor ISA-2011B had no significant effect (Fig. 4 C, D). This indicates that the stimulation of neurite outgrowth and progenitor proliferation by Marcks and Marcksl1 is indeed PIP_2 dependent. While PIP_2 is generally thought to act upstream of PLD, additional experiments will be needed to confirm this for the developing spinal cord.

The ability of Marcks to promote PIP_2 signaling has been previously suggested to be linked to the subcellular localization of the protein, which depends on its phosphorylation status, with unphosphorylated Marcks being mostly membrane-bound and phosphorylated Marcks being largely cytoplasmic (Kim et al., 1994, McLaughlin & Aderem, 1995). In turn, the phosphorylation status of Marcks is regulated by Protein kinase C (PKC) (McLaughlin & Aderem, 1995). Although Marcks and Marcksl proteins are severely depleted in our CRISPR-injected embryos, clones of cells with at least partially functional Marcks and Marcksl proteins are expected to be present due to the mosaicism of CRISPR knockout effects in our F0 embryos. Assuming that subcellular localization of Marcks and Marcksl1 is functionally important in the spinal cord, we should thus be able to partially rescue the deficiencies of our CRISPR embryos by modulating PKC activity.

To test this hypothesis, we used the potent PKC activator Phorbol 12-myristate 13-acetate (PMA) and the broad-spectrum PKC inhibitor Go6983 (Liu & Heckman, 1998, Shen, 2003). Compared to DMSO-treated controls, embryos treated with the PKC inhibitor Go6983 showed a significant increase in the intensity of acetylated tubulin staining (Fig. 4 E) as well as in the proportion of PH3-positive cells (Fig. 4 F) on the CRISPR-injected side relative to the uninjected side. In contrast, the PKC activator PMA had no significant effect (Fig. 4 E, F). These findings suggest that the unphosphorylated, presumably membrane-bound fraction of Marcks and Marcksl1 is primarily required for neurite outgrowth and progenitor proliferation in the spinal cord. Our other findings suggest that membrane-bound Marcks and Marcksl1 may promote these processes via the activation of PIP_2-mediated PLD signaling. However, the hierarchy of these interactions needs to be confirmed in future studies.

Expression of Marcks and Marcksl1 during spinal cord regeneration in uninjected tadpoles and after 4M CRISPR knockout

309 After complete transection of the spinal cord, tadpoles of *Xenopus laevis* have previously
310 been shown to close the injury gap with cells and regenerating neurites at around ten days post
311 transection (DPT), with almost full functional recovery at 20 DPT (Lee-Liu et al., 2014, Munoz
312 et al., 2015, Edwards-Faret et al., 2018). Because Marcks and Marcksl1 were identified in a
313 proteomic screen for proteins differentially upregulated after spinal cord injury (SCI) in
314 regeneration-competent tadpoles (Kshirsagar, 2020), we next focused on the role of these
315 proteins during spinal cord regeneration in *Xenopus*.
316 For these experiments, *marcks.L/S* and *marcksl1.L/S* sgRNAs (4M CRISPR) were injected
317 into 1-cell stage embryos, which were then raised to stage 50 tadpoles (Fig. 5 A). After
318 removing some dorsal skin, muscle, and meninges, the spinal cord was transected entirely at a
319 mid-thoracic level. Sham-injured tadpoles were treated the same way but without transection
320 of the spinal cord. Tadpoles were screened before SCI and at 2-, 5-, and 10-days post
321 transection (DPT) for swimming capacity and some tadpoles at each time point were fixed,
322 cryosectioned and evaluated by assessing the distribution of neurites (acetylated tubulin+) and
323 measuring spinal cord gap closure length as well as percentages of proliferating cells (EdU+)
324 and neuro-glial progenitor cells (Sox2+) (Fig. 5 A).
325 We first analyzed the distribution of Marcks and Marcksl1 in the uninjured spinal cord and
326 at 2-, 5-, and 10-DPT in normal (uninjected) and 4M CRISPR-injected tadpoles. In uninjected,
327 uninjured tadpoles, Marcks protein was detected primarily in the meningeal layer surrounding
328 the spinal cord, with relatively little immunostaining in the spinal cord itself (Fig. 5 B-D).
329 Barely any Marcks protein was detectable in uninjured 4M CRISPR tadpoles (Fig. 5 N, O). At
330 2 DPT, the levels of Marcks protein in the meninges and spinal cord remain relatively
331 unchanged in both normal (Fig. 5 E-G) and CRISPR-injected (Fig. 5 P, Q) tadpoles. However,
332 additional Marcks staining was observed in normal tadpoles in cells within the injury gap (Fig.
333 5 E-G). At 5 DPT, normal tadpoles showed an apparent upregulation of Marcks in all layers of
334 the spinal cord adjacent to the injury site, including the ventricular zone, where neuro-glial
335 progenitors reside, the mantle zone, which harbors differentiated neurons, and the marginal
336 zone, occupied by neurites (Fig. 5 H-J). Marcks also continues to be elevated in cells in the
337 region of the injury gap, which is about to close (Fig. 5 H-J). This pattern of elevated Marcks
338 staining was maintained at 10 DPT (Fig. 5 K-M). In contrast, 4M CRISPR tadpoles showed no
339 significant increases of Marcks immunostaining in the spinal cord or adjacent tissues at 5- and
340 10-DPT (Fig. 5 R-U).
341 Compared to Marcks, Marcksl1 showed slightly stronger immunostaining in the spinal cord
342 and weaker staining in the meninges of uninjected uninjured tadpoles but less pronounced

343 upregulation after SCI (Fig. S14 A-L). As described for Marcks, Marcksl1-immunopositive
344 cells also accumulated within the injury gap from 2 DPT onwards (Fig. S14 D-L). Again,
345 almost no Marcksl1 immunostaining was detectable in 4M CRISPR tadpoles in and around the
346 spinal cord before the injury, and no significant changes were observed following SCI (Fig.
347 S14 M-T). Patterns of Marcks and Marcksl1 immunostaining for sham-operated tadpoles
348 resembled those observed in uninjected and uninjured tadpoles and did not change at days 2-
349 10 post-injury (Fig. S15). Taken together; these observations suggest that Marcks and Marcksl1
350 are present at low levels in the tadpole spinal cord but become upregulated in all layers of the
351 spinal cord next to the injury site after SCI (in particular, Marcks), while Marcks- and
352 Marcksl1-immunopositive cells infiltrate the lesion site.
353

354 ***Marcks and Marcksl are required for functional recovery after spinal cord transections in***
355 ***Xenopus tadpoles***

356 To further elucidate the role of Marcks and Marcksl1 in spinal cord regeneration, we next
357 used a behavioral test to analyze whether functional recovery after SCI is impaired in 4M
358 CRISPR tadpoles compared to normal (uninjected) tadpoles. Tadpoles were put into 6-well
359 plates equipped with an intermittently vibrating motor to stimulate movement and were video
360 recorded for 1.5 minutes. Their total swimming distances were then calculated from the videos.
361 The distances covered by uninjected and 4M CRISPR-injected uninjured tadpoles were not
362 significantly different (Fig. 6 A). This, together with our histological data described below,
363 suggests that while the CRISPR knockout of Marcks and Marcksl1 perturbs axon outgrowth
364 and cell proliferation during normal development, ultimately, these tadpoles develop a
365 relatively normally functioning spinal cord. Following SCI, there is a significant decrease in
366 swimming distances at 2 and 5 DPT with no significant difference between uninjected and
367 CRISPR animals (Fig. 6 A, Fig. S16 A).
368 However, at 10 DPT, the average swimming distance of uninjected tadpoles had recovered
369 to a level not significantly different from pre-injury levels. In contrast, the average swimming
370 distance of 10 DPT CRISPR tadpoles was significantly shorter (Fig. 6 A, Fig. S16 A). Animals
371 with sham surgeries showed no significant changes in swimming distances compared to
372 uninjected and uninjured tadpoles over time (Fig. S16 B), suggesting that spinal cord
373 transection alone accounts for these behavioral differences. This indicates that the CRISPR
374 knockout of Marcks and Marcksl1 significantly delays the capacity of tadpoles to recover
375 functionally after SCI, supporting the vital role of these proteins for spinal cord regeneration.

376

377 ***Marcks and Marcksl1 are required for injury gap closure and proliferation of neuro-glial***
378 ***progenitors during spinal cord regeneration***

379

380 We next used immunostaining with acetylated tubulin and DAPI nuclear staining to analyze
381 how Marcks and Marcksl1 knockout affects the regrowth of neurites and injury gap closure
382 (measured as the distance between the DAPI+ ventricular zones of rostral and caudal stump)
383 after SCI. Horizontal sections of the spinal cords of uninjured 4M CRISPR-injected animals
384 resembled those of uninjured animals with prominent and well-distinguished ventricular,
385 mantle, and marginal zones (Fig. 6 B, F). This demonstrates that the CRISPR-induced defects
386 during spinal cord development described above only delay but ultimately do not prevent the
387 formation of an adequately organized spinal cord, allowing the use of these animals for spinal
388 cord regeneration studies.

389 After SCI, the length of the injury gap is initially similar for uninjected and 4M CRISPR-
390 injected tadpoles (Fig. 6 C, G, J). However, at 5 DPT, the first axonal bridges seem to form
391 and connect the rostral and caudal stumps in the uninjected animals, which is delayed until 10
392 DPT in the CRISPR tadpoles (Fig. 6 D, E, H, I). Moreover, while the injury gap decreased over
393 time in both uninjected and 4M CRISPR-injected tadpoles, the injury gap at 5- and 10- DPT in
394 4M CRISPR-injected remained significantly larger than in uninjected embryos, indicating a
395 delay in regenerative closure (Fig. 6 D, E, H, I, J).

396 To determine the effects of Marcks and Marcksl1 knockout on cell proliferation during
397 spinal cord regeneration, EdU was injected into the tadpoles 16 hours before the analysis
398 timepoint to achieve saturated labeling of the entire population of proliferating cells. DAPI-
399 stained nuclei and EdU+ nuclei were then counted in a defined window across the injury site
400 (i.e., the area shown in each of the panels of Fig. 7). There was no significant difference
401 between uninjured uninjected and 4M CRISPR-injected animals (Fig. 7 A1, B1, A2, B2, I). In
402 response to SCI, then a significant increase in the proportion of EdU+ cells was observed in
403 uninjected tadpoles at 2- and 5- DPT, which returned to pre-injury levels at 10 DPT (Fig. 7 A1-
404 H1, I, Fig. S17 A). An increase in EdU+ cell numbers was seen in the ventricular zone and
405 cells in and adjacent to the injury gap (Fig. 7 C1-F1). Sham-operated animals showed no
406 significant changes in EdU+ cells over time (Fig. S18 B), indicating that these changes occur
407 only after spinal cord transection. In contrast, there was no significant change in the proportion
408 of EdU+ cells in the 4M CRISPR-injected tadpoles after SCI (Fig. 7 A2-H2, I, Fig. S17 A).

To test whether Marcks and Marcksl1 also affect the distribution and numbers of neuro-glial progenitors during spinal cord regeneration, we then visualized and quantified Sox2-immunopositive cells after SCI. Again, the distribution of Sox2+ cells in the ventricular zone was similar, and there was no significant difference between uninjured uninjected and 4M CRISPR-injected animals (Fig. 8 A1, B1, A2, B2, I).

In uninjected tadpoles at 2 and 5 DPT, we observed an increase in Sox2+ cell numbers rostral to the injury site of the transected spinal cord (Fig. 8 C1-F1). However, near the injury, Sox2+ cells were reduced (particularly at 2 DPT). This was reflected in a slight decrease in the number of Sox2+ cells counted in our standard window around the injury site (Fig. 8 I). However, at 10 DPT, Sox2+ cells were noticeably and significantly increased in the entire ventricular zone of the regenerating spinal cord, both rostral and caudal of the injury site (Fig. 8 G1, H1, I). Again, animals with sham surgeries did not show any significant changes in the population of Sox2+ cells (Fig. S18 B), indicating that the observed changes occur only after spinal cord transection.

In the 4M CRISPR-injected tadpoles, there was a slight overall decrease in Sox2+ cells at 2- and 5-DPT, similar to the uninjected tadpoles (Fig. 8 C2-F2, I). However, in contrast to the uninjected tadpoles, the CRISPR tadpoles did not show any elevation of Sox2+ immunostaining in the rostral spinal cord, and there was no overall increase in Sox2+ cell numbers at 10 DPT, with Sox2+ counts significantly decreased compared to uninjected tadpoles (Fig. 8 G2, H2, I). Taken together, our findings show that after SCI Marcks and Marcksl1 are required for multiple processes implicated in spinal cord regeneration (Lee-Liu et al., 2013, Alunni & Bally-Cuif, 2016, Rodemer et al., 2020), including neurite outgrowth and the proliferation and possibly maintenance of neuro-glial progenitors in the ventricular zone.

The PLD signaling pathway mediates Marcks and Marcksl1 functions during spinal cord regeneration

Since we found PLD signaling to be involved in mediating the effects of Marcks and Marcks1 on axon outgrowth and proliferation of neuro-glial progenitors during normal spinal cord development, we next asked whether the role of Marcks and Marcks1 for spinal cord regeneration may also be modulated by PLD activity. 4M CRISPR-injected tadpoles with spinal cord injury were exposed to the PLD activator S1P, the PLD inhibitor FIPI, or only DMSO in control embryos for seven days. At 7 DPT, the tadpoles were then compared for

behavioral recovery, injury gap closure, and EdU+ and Sox2+ cell numbers (Fig. 9). The swimming recovery test revealed that tadpoles exposed to the PLD activator S1P swam significantly longer distances than control animals (Fig. 9 P). Conversely, tadpoles exposed to the PLD inhibitor FIPI traveled a shorter distance than the DMSO controls, but this difference was insignificant (Fig. 9 P). Immunostaining for acetylated tubulin combined with nuclear DAPI staining showed that injury gap length was significantly reduced in animals incubated in the PLD activator S1P. In contrast, it was significantly higher in the animals incubated in the PLD inhibitor FIPI (Fig. 9 A-C, Q). The proportion of proliferative EdU+ cells (Fig. 9 D-I, R) and of Sox2+ neuro-glial progenitor cells (Fig. 9 J-O, S) was also significantly increased in the tadpoles incubated in the PLD activator S1P and significantly decreased in those exposed to the PLD inhibitor FIPI compared to DMSO controls. Thus, in all parameters investigated, 4M CRISPR tadpoles treated with PLD activators adopted a phenotype resembling normal tadpoles after SCI. In contrast, those treated with PLD inhibitors showed more severe loss of function phenotypes than untreated CRISPR tadpoles.

This shows that PLD activation can rescue the delaying effects of Marcks and Marcksl1 knockout on functional recovery, injury gap closure, and proliferation of neuro-glial progenitors after SCI, while PLD inhibition further exacerbates them. This suggests that the functions of Marcks and Marcksl1 during spinal cord regeneration are partially mediated by PLD, similar to their roles in normal spinal cord development.

Discussion

The upregulation of Marcks and Marcksl1 proteins after SCI in the regenerating spinal cord of *Xenopus* tadpoles, but their downregulation in the non-regenerative spinal cord of froglets (Kshirsagar, 2020) led us to investigate the role of these proteins during normal spinal cord development as well as during spinal cord regeneration. Our findings indicate that these proteins act redundantly and are required for normal neurite outgrowth, proliferation, and possibly the maintenance of neuro-glial progenitor cells during spinal cord development. However, a reasonably normal spinal cord will eventually develop after the knockdown or knockout of both proteins, suggesting that Marcks- and Marcksl1-independent mechanisms can subsequently compensate for the loss of these proteins.

We also demonstrated that Marcks and Marcksl1 play similar roles in spinal cord regeneration in tadpoles after injury. Neurite outgrowth, injury gap closure, activation of proliferation, and increase in the number of Sox2+ neuro-glial progenitors near the injury site

476 were drastically reduced in tadpoles after the knockout of both proteins and functional recovery
477 of swimming was delayed. The upregulation of proliferating Sox2+ cells in the ventricular zone
478 was previously shown to be required for regeneration, suggesting that increased division and
479 migration of these cells contribute to injury gap closure and the generation of a permissive
480 environment for neurite regrowth (Gaete et al., 2012; Munoz et al., 2015).

481 Our finding that Marcks and, to a lesser extent, Macksl1 are upregulated in the entire spinal
482 cord, including the ventricular zone, as well as in cells filling the injury gap, suggests that these
483 proteins may act cell-autonomously in the spinal cord-derived cells to promote these
484 regenerative processes. This is also supported by a recent single-cell RNA-seq study of
485 regenerating *Xenopus* tails, which showed that Marcks and Marcksl1 are highly enriched in
486 many neural cell types during tail regeneration (Aztekin et al., 2019). However, since both
487 proteins are known to be expressed in macrophages and other immune cells and can modulate
488 the inflammatory response (Carballo, Pitterle, Stumpo, Sperling, & Blackshear, 1999, El Amri
489 et al., 2018; Zhou & Li, 2000), Marcks- and Marcksl1-immunopositive immune cells that
490 infiltrate the injury site may also contribute to the regeneration-promoting effects of these
491 proteins. Double-labeling with cell type-specific markers and single-cell RNA-seq following
492 SCI will be required in the future to clarify the relative contribution of different Marcks- and
493 Marcksl1-expressing cell types to spinal cord regeneration.

494 We also show here that a specific PLD activator can rescue deficiencies of neurite outgrowth
495 and neuro-glial progenitor proliferation after the knockdown of Marcks and Marcksl1 during
496 spinal cord development and regeneration. In contrast, a specific PLD inhibitor further
497 enhances these deficiencies after SCI. Taken together with our findings that enhancement of
498 PIP_2 synthesis and inhibition of PKC is also able to rescue the effects of Marcks and Marcksl1
499 knockout during spinal cord development, this is compatible with a model in which
500 unphosphorylated, membrane-bound Marcks promotes neurite outgrowth and progenitor
501 proliferation via PIP_2 dependent activation of PLD signaling (Fig. 9 T). This is in agreement
502 with previous studies showing that unphosphorylated membrane-bound Marcks promotes
503 neurite outgrowth by modulating PIP_2 signaling due to its ability to sequester PIP_2 in membrane
504 rafts (Laux et al., 2000), thereby potentially stimulating PIP_2 signaling (Trovo et al., 2013) but
505 see (Laux et al., 2000). It also provides a link to previous studies suggesting an essential role
506 of PLD-dependent mTORC1 signaling for the proliferation of neuro-glial progenitors during
507 spinal cord regeneration (Sun & Chen, 2008, Kanno et al., 2012, Penailillo et al., 2021).
508 However, additional experiments are needed to corroborate the various specific interactions
509 implied by this model.

510 In conclusion, our present study reveals a hitherto unrecognized essential function of
511 Marcks and Marcksl1 for spinal cord development and regeneration, highlighting the potential
512 of *Xenopus* as a model system for regeneration studies and suggesting new pathways to be
513 targeted for therapeutic stimulation of spinal cord regeneration in human patients.
514
515

516 **Materials and Methods**

517 **Animals**

518 Frogs (*Xenopus laevis*) were obtained from a commercial breeder (Xenopus One Corp,
519 Michigan, USA). All experiments were done in accordance with Irish and European
520 legislation under licenses AE19125/P079 and AE19125/P098 from the Health Products
521 Regulatory Authority (HPRA).

522 **Morpholino Antisense Oligonucleotides (MO)**

523 Translation-blocking MOs, and a standard control MO (5′-CCTCTTACCTCAGTTACAA
524 TTTATA-3′) were obtained from Gene Tools. *Xenopus laevis* is an allotetraploid (Session et
525 al., 2016) and its genome contains two homeologs (denoted.L and.S, respectively) of many
526 genes, including *marcks* and *marcksl1*. Therefore, in our functional studies, we designed MOs
527 to block both homeologs. The marcks MO (5'-GGTCTTGGAGAATTGGGCTCCCA TT-3')
528 (Iioka, Ueno, & Kinoshita, 2004) target base pairs -16 to +9 of both *marcks.S* and *marcks.L*.
529 The marcksl1.L MO (5'-GGATTCTATACTACCCATTTTCCGC-3') targets base pairs -7 to
530 +18 of *marcksl1.L*, while the marcksl1.S MO (5'- GGACTCTACGCTACCCATTGTGACT-
531 3') (Zhao, Cao, & Grunz, 2001) targets base pairs -2 to +23 of *marcksl1.S*.
532 The efficacy of all MOs was verified in western blots following in vitro transcription and
533 translation (TNT-coupled Wheat Germ Extract kit, Promega) of pCMV-Sport6-marcks.S,
534 pCMV-Sport6-marcksl1.S, and pCMV-Sport6.ccdb-marcksl1.L (1 µg/50 µl reaction) with and
535 without MO (20 pg marcksl1.L MO or 40 pg of marcksL1.S or marcks.S MOs /50 µl reaction)
536 as previously described (Ahrens & Schlosser, 2005). 2 µl biotinylated Transcend tRNA
537 (Promega) was included in the reaction mix resulting in biotinylation of lysine residues. PVDF
538 membranes were subsequently incubated with Streptavidin Alkaline Phosphatase (1:5000;
539 Promega) to visualize proteins in Transcend Chemiluminescence Substrate (Promega). The
540 specificity of all MOs was verified by co-injection with the rescue mRNAs (see below).
541

542 **Expression Constructs**

543 Plasmids encoding membrane-GFP (pCS2+-memGFP) and c-myc-GFP (pCMTEGFP)
544 were provided by John Wallingford (Wallingford et al., 2000) and Doris Wedlich, respectively.
545 cDNA clones for *Xenopus laevis* marcks.S (clone accession: BC041207), marcks.L (clone
546 accession: BC084888), and marcksl1.S (clone accession: BC157454) were purchased from
547 Source Bioscience, provided in pCMV-Sport6 backbone vectors and pCMV-Sport6.ccdb for
548 *marcksl1.L*. Due to a nucleotide sequence identity of 94% between *marcks.L* and *marcks.S*,
549 only the cDNA clone for *marcks.S* was used. All plasmids were verified by sequencing and
550 linearized with ClaI before mRNA synthesis using the SP6 Ambion Message Machine™ Kit
551 (Invitrogen).

552 For rescue experiments, chicken *marcks* (clone ID: OGa33947C) and *Xenopus tropicalis*
553 *marcksl1* (clone ID: OXa00945C) ORF clones were purchased from GenScript (GenBank
554 accession numbers: NM_001044437.1; XM_015284506.2). The clones were received in pET-
555 23a(+) vectors, containing a His-tag and T7-tag, flanking the cloning sites on each terminal.
556 There were 3/25 base-pair mismatches between Xl-Marcks.S MO and the pET-23a(+)-
557 marcks_OGa33947C sequence; 9/25 mismatches between Xl-Marcksl1.L MO and pET-
558 23a(+)-marcksl1_OXa00945C; and 10/25 mismatches between Xl-Marcksl1.S MO and pET-
559 23a(+)-marcksl1_OXa00945C. To increase the number of mismatches between the MOs and
560 the mRNA rescue constructs, seven and eight additional substitutions were introduced into
561 pET-23a(+)-marcks_OGa33947C and pET-23a(+)-marcksl1_OXa00945C_plasmids,
562 respectively, using the Q5 site-directed mutagenesis kit (New England Biolabs). These
563 substitutions did not alter protein sequences. For mutagenesis, forward (5'-
564 TTTAGTAAAACAGCTGCGAAGGGCGAAGCC-3') and reverse (5'-
565 CTGTGCACCCATGGATCCGCGACCCATTTGC-3') primers for pET-23a(+)-
566 marcks_OGa33947C were annealed at 70 °C, while forward (5'-
567 ATCGAGAGTAAGTCTAAGAGTGCAGATATTAGC-3') and reverse (5'
568 GGAGCCCATGGATCCGCGACCCATTTG-3') primers for pET-23a(+)-
569 marcksl1_OXa00945C were annealed at 63 °C. Mutagenized plasmids were verified by
570 sequencing and linearized with AdeI before mRNA synthesis using the T7 Ambion Message
571 Machine Kit (Invitrogen), followed by polyadenylation using the Poly(A) Tailing Kit
572 (Invitrogen).

573

574 **CRISPR/Cas9-based Gene Editing**

575 *marcks.L/S* and *marcksl1.L/S* genomic sequences were derived from the most recent version
576 of the *Xenopus laevis* genome on Xenbase (https://www.xenbase.org/) and NCBI
577 (https://www.ncbi.nlm.nih.gov/genome/). Two single-guide RNA primers targeting the first
578 exon of *marcks.L/S* (5'-
579 CTAGCTAATACGACTCACTATAGGCTGCGGTCTTGGAGAATTGTTTTAGAGCTAG
580 AAATAGCAAG-3') and second exon of *marcksl1.L/S* (5'-
581 CTAGCTAATACGACTCACTATAGGTTGGGGTCCCCGTTGGCGGTTTTAGAGCTAG
582 AAATAGCAAG-3'), respectively (target specific region underlined), were designed using
583 CRISPRscan (https://www.crisprscan.org). These gene-specific sgRNA primers contained a
584 T7 promoter site (TAATACGACTCACTATA) with five additional nucleotides in the 5' end
585 for enhanced transcriptional output, two guanines for in vitro transcript yield efficiency, 17-18
586 nucleotides encoding the target-specific region (underlined), and a 23-nucleotide tail for
587 annealing to the 80-nucleotide universal reverse primer (5'-
588 AAAAGCACCGACTCGGTGCCACTTTTTCAAGTTGATAACGGACTAGCCTTATTTT
589 AACTTGCTATTTCTAGCTCTAAAAC-3'). As a control, an sgRNA targeting *solute carrier*
590 *family 45 member 2* (*slc45a2*) 5'-
591 CTAGCTAATACGACTCACTATAGGTTACATAGGCTGCCTCCAGTTTTAGAGCTAG
592 AAATAGCAAG-3'), encoding a protein that mediates melanin synthesis, was used (DeLay et
593 al., 2018). In *X. laevis*, *slc45a2* is present as only one homeolog, *slc45a2.L*. Off-target, and
594 editing efficiency probabilities were assessed using InDelphi
595 (https://indelphi.giffordlab.mit.edu/), GGGenome (https://gggenome.dbcls.hp/) and
596 CRISPRscan.
597 sgRNAs were synthesized (Bhattacharya, Marfo, Li, Lane, & Khokha, 2015) using PCR
598 with Q5 High-Fidelity DNA Polymerase (NEB), 1 µM each of forward and reverse primer and
599 the following cycling conditions: 98 °C for 30 seconds; 10 cycles of 98 °C for 10 seconds, 62
600 °C for 20 seconds, 72 °C for 20 seconds; 25 cycles of 98 °C for 10 seconds, 72 °C for 30
601 seconds; and 72 °C for 5 minutes. PCR products were purified using the DNA Clean &
602 Concentrator-5 (Zymo Research, D4014) and in vitro transcribed using the MEGAshortscript
603 T7 Transcription Kit (Invitrogen). After a 4-hour incubation at 37 °C and subsequent TURBO
604 DNase treatment for 15 minutes, the sgRNA was purified using the GeneJET RNA Cleanup
605 and Concentration Micro Kit (Thermo Scientific) in accordance with the manufacturer's
606 protocol with the following modifications: The transcription reaction mixture was first adjusted
607 to 50 µl with nuclease-free water, followed by the addition of 250 µl of Binding Buffer. After

608 elution in nuclease-free water, the concentration of sgRNAs was adjusted to 500 ng/µl, and
609 aliquots were stored at -80 °C.

610

611 **Microinjections**

612 Embryos of *Xenopus laevis* were staged according to (Nieuwkoop & Faber, 1967) and injected
613 according to standard procedures (Sive, Grainger, & Harland, 2000). mRNAs were injected
614 into single blastomeres at the 2- to 8-cell stage, giving rise to the dorsal ectoderm. To visualize
615 membranes in confocal microscopy, *mem-GFP* mRNA was injected (125 pg). For the
616 overexpression study, 100 or 300 pg of *marcks* or *marcksl1* mRNA was co-injected with 125
617 pg *myc-GFP* mRNA to identify the injected side. As a control, only *myc-GFP* mRNA (125 pg)
618 was injected. Morpholinos (see above) were injected singly or as a cocktail (9 ng each) with
619 125 pg c-*myc*-GFP mRNA. 27 ng of the standard control MO was used in control injections.
620 For MO rescue experiments, 300 pg mutated chicken *marcks* mRNA and 350 pg mutated
621 *Xenopus tropicalis marcksl* mRNA was co-injected with 9 ng of each MO. For CRISPR/Cas9
622 experiments, embryos were injected with a ribonucleoprotein (RNP) mix containing 500 pg of
623 each sgRNA, 1 ng TrueCut Cas9 Protein v2 (Invitrogen, A36497), and 125 pg *myc-GFP*
624 mRNA. The RNP mix was incubated at room temperature for at least 10 min before injection.

625

626 **Extraction and Analysis of Genomic DNA**

627 Approximately five days after the injection of RNPs, genomic DNA was extracted from
628 embryos using the Wizard Genomic DNA Purification Kit (Promega) according to the
629 manufacturer's Animal Tissue protocol. Upon extraction, the DNA was rehydrated in 25 µl of
630 DNA Rehydration Solution overnight at 4°C. CRISPR-targeted regions in *marcks.L/S* and
631 *marcksl1.L/S* were PCR-amplified using the EmeraldAmp GT PCR Master Mix (Takara Bio).
632 For every gene, each 40 µl reaction contained 20 µl of 2X EmeraldAmp Master Mix, 1 µl of
633 the forward and reverse primer mix diluted to 10 µM, 100 ng of genomic template DNA, and
634 PCR-grade H_2O for volume adjustment. The cycling conditions were 98 °C for 30 seconds, 30
635 cycles of 98 °C for 10 seconds, 60 °C for 30 seconds, 72 °C for 1 minute per kilobase of PCR
636 product, and 72 °C for 5 minutes. The following forward (F) and reverse (R) primer pairs were
637 used: *marcks.L* (F: 5'-ATCACCTGATGGACGCATGG-3', R: 5'-
638 CCCCCACATCTAAAGCGGAG-3'), *marcks.S* (F: 5'-AGTGTCATGAATCAGCGGGG-3',
639 R: 5'-GTGTGTCTATTAGCGGCGGA-3'), *marcksl1.L* (F: 5'-

640 GCTAGGAAGAAGCGAGTCCC-3', R: 5'-ACCCGTTAACATGAGCAGCA-3'),
641 *marcksl1.S* (F: 5'-AGAAAGAAGTGAGCCTAGAGTGATT-3', R: 5'-
642 ATCCCTCCAAGGGTGACAGG-3'), *slc45a2.L* (F: 5'-GTTCCCTTCGCTCATACAATG-
643 3', R: 5'-GCCAGAAAGGGGTTTATTGC-3'). 5 µl of each PCR product was run in a 1%
644 agarose gel and the remaining 35 µls were purified using the QIAquick PCR Purification Kit
645 (Qiagen) before being sent for sequencing (sequencing primers: *marcks.L*: 5'-
646 CCCATGCTGTCTGTCTTTGA-3', *marcks.S*: 5'-GTGTGTCTATTAGCGGCGGA-3',
647 *marcksl1.L*: 5'-TCTTCTTCTGGCGCCTGC-3', *marcksl1.S*: 5'-
648 AGTTTAGGGAGGCAGGGTTG-3', *slc45a2.L*: 5'-GTTCCCTTCGCTCATACAATG-3').
649 Sequencing raw data from wild-type, *slc45a2*, and *marcks/marcksl1*-targeted embryos were
650 analyzed for the frequency of insertion/deletion mutations using the Synthego ICE algorithm
651 (https://ice.synthego.com/) (Conant et al., 2022).
652

653 **Antibodies**

654 Affinity-purified polyclonal antibodies against *Xenopus* Marcks and Marcksl1 proteins were
655 generated by the company GenScript. For anti-Marcks, a His-tagged fusion protein with the
656 following sequence was expressed in bacteria:
657 MHHHHHHASPAEGEPAEPASPAEGEPAAKTEEAGSTSTPSTSNETPKKKKKRFSFKK
658 SFKLSGFSFKKNKKENSEGAENEGA. Using the Protein BLAST NCBI tool, this
659 immunogen (including the 6-His-tag) shared a 98.68 percent identity (E value: 3e-43) with
660 Marcks.L (NCBI Reference Sequence XP_018118779.1) and 98.67% (E value: 3e-42) with
661 Marcks.S (XP_018119725.1). No other sequences in *X. laevis* (taxonomy id:8355) returned
662 any significant alignments. The protein was purified in Nickel and Superdex 75 columns and,
663 after LC-MS validation, was used to immunize rabbits. The antibody was then antigen-affinity-
664 purified from sera and tested by indirect ELISA by Genscript. For anti-Marcksl1, keyhole
665 limpet hemocyanin (KLH)-tagged peptides (CGDPKPEDPPGKQAK) were used to immunize
666 rabbits and were affinity-purified. This peptide had a 100% sequence identity (E value: 6e-08)
667 with both Marcksl1.L (NP_001108274.1) and Marcksl1.S (NP_001081982.2). The next closest
668 sequence alignments returned insignificant E values greater than 0.34.
669

670 **Histochemistry**

671 Embryos and tadpoles were fixed in 4% PFA in 0.1 M phosphate buffer (PB) overnight,
672 followed by two washes in PB for 10 minutes, before cryoprotection in 20% sucrose/PB
673 overnight at 4°C. The specimens were then positioned in rubber forms and embedded in O.C.T.
674 (VWR) for 30 minutes before shock-freezing in 2-Methylbutane cooled in liquid nitrogen.
675 Immunohistochemistry on 20 µm cryosections was performed as previously described
676 (Schlosser & Ahrens, 2004). Primary antibodies were diluted, as indicated in Table 1. The
677 following secondary antibodies were used at 1:500 dilution supplemented with DAPI (100
678 ng/µl): Alexa Fluor 488- and Alexa Fluor 594-conjugated goat anti-mouse (Invitrogen A11001
679 and A11005, respectively); Alexa Fluor 488- and Alexa Fluor 594-conjugated goat anti-rabbit
680 (Invitrogen A11008 and A11012, respectively); and Alexa Fluor 594-conjugated donkey anti-
681 mouse and anti-rabbit (Invitrogen A21203 or A21207, respectively).
682 Incorporation and histochemical detection of 5-ethynyl-2′-deoxyuridine (EdU) was used to
683 label the entire proliferating cell population before and after spinal cord injury. EdU was
684 initially diluted to 5 mg/ml in 0.8x PBS, followed by 5 µl intracoelomic injections into tadpoles
685 16 hours before the desired time point (Edwards-Faret et al., 2017). In tadpole cryosections
686 immunostained for Sox2, EdU was detected after secondary antibody incubation using the
687 Click-iT™ EdU Cell Proliferation Kit for Imaging and Alexa Fluor 488 dye (Invitrogen).
688

689 **In situ Hybridization**

690 After fixation in 4% paraformaldehyde, whole-mount in situ hybridization was carried out
691 as previously described (Schlosser & Ahrens, 2004). pcMV-Sport6-marcks.S, pCMV-Sport6-
692 marcksl1.S, and pCMV-Sport6.ccdb-marcksl1.L were linearized with EcoRV followed by
693 synthesis of anti-sense RNA probes using the digoxigenin RNA Labeling Kit (Sigma Aldrich)
694 and SP6 polymerase. Vibratome sections (40 µm) were cut after the whole-mount in situ
695 hybridization.
696

697 **Pharmacological Assays**

698 Uninjected and RNP-injected embryos (see above) were incubated in various chemical
699 compounds three days post-fertilization for 24 hours at 14 °C in a dark incubator. All
700 compounds were solubilized in DMSO and diluted in 0.1X MBS (Sive et al., 2000). Control
701 embryos were incubated in 2% DMSO/0.1X MBS. The medium was changed once after 12
702 hours of incubation in a 12-well plate (6 embryos per well). To determine the proper dosage, a

703 dose-titration screening was first conducted for all chemicals using dilutions of 0.01 μM, 0.1
704 μM, 1 μM, and 10 μM in DMSO. The highest dose that produced comparable mortality rates
705 to the DMSO control embryos was selected for further studies. Sphingosine-1-phosphate (S1P)
706 (1 μM, TOCRIS) and 5-Fluoro-2-indolyl des-chlorohalopemide (FIPI) (10 μM, TOCRIS) were
707 used to activate and inhibit PLD, respectively. NMI (10 μM, TOCRIS) and ISA-2011B (10
708 μM, MedChemExpress) enhanced or inhibited phosphatidylinositol biosynthesis, respectively.
709 Finally, Phorbol 12-myristate 13-acetate (PMA) (0.01 μM, TOCRIS) and Go 6983 (10 μM,
710 TOCRIS) were used to activate or inhibit PKC, respectively.

711

712 **Imaging and Statistical Analysis**

713 Immunostained cryosections and vibratome sections were visualized using an Olympus
714 BX51 fluorescence microscope and recorded with an Olympus DP72 camera. Some
715 representative images were obtained by confocal microscopy (Olympus Fluoview 1000
716 Confocal Microscope). For each epitope, images were acquired using identical exposure
717 settings for signal threshold determination and balancing. Representative images were flipped
718 and/or cropped with contrast adjustments to highlight biological relevance using Image J
719 (National Institutes of Health).
720 To quantify acetylated tubulin integrated density, the injected and uninjected areas of every
721 second consecutive spinal cord section were manually selected using the freehand selection
722 tool and measured in ImageJ. At least eight transverse 20 μm sections were analyzed per
723 animal, spanning the length of more than 300 μm in developing spinal cords. The integrated
724 density for the injected and uninjected sides was averaged separately for every animal. Then,
725 a ratio for these averages – the integrated density ratio (IDR) - was calculated for every animal.
726 To determine Sox2/3-positive cell numbers, individual cells from at least eight alternating
727 serial sections were counted on the injected and uninjected sides. For every animal, the ratio
728 for the average number of cells in the injected to uninjected sides was calculated. The
729 percentage of PH3+ cell nuclei out of all ependymal DAPI-positive nuclei was calculated for
730 quantification of cell division on the injected and uninjected sides. For every animal, the ratio
731 for the percentage of PH3+ cell nuclei in the injected to uninjected sides was calculated. After
732 SCI, at least five horizontal spinal cord 20 μm sections were obtained per animal and condition.
733 The length between the regenerating stumps was calculated using Image J, and averaged for
734 every animal. Total cell counts from DAPI, EdU, and Sox2 images were also determined using

735 Image J. DAPI-stained nuclei and EdU+ nuclei were counted in at least five horizontal sections
736 per animal. Within each section, the entire population of cells in the spinal cord in a window
737 extending 330 µm across the spinal cord and extending for 440 µm along the anteroposterior
738 axis across the injury site and including the rostral and caudal stumps was analyzed (i.e., the
739 area depicted in each of the panels of Fig. 7). After binary conversion and particle analysis in
740 ImageJ, the percentage of EdU+ or Sox2+ cells over the entire nuclear cell count was
741 calculated.

742 Several statistical tests were employed for this study using GraphPad Prism (San Diego,
743 California). A one-way ANOVA was chosen to compare how a single variable, MOs or RNPs,
744 could affect neurite outgrowth or cell proliferation. The mean of each condition was then
745 compared using the Tukey test, which compares every mean with every other mean. For
746 pharmacological treatments on developing embryos, a one-way ANOVA was also used with a
747 Dunnett test to compare every mean to a control mean, which was the DMSO condition. A 2-
748 way ANOVA was used to compare how CRISPR-gene disruption and injury time points can
749 affect gap closure length after SCI. Here, an uncorrected Fisher's least significant difference
750 (LSD) test was used for pairwise comparisons of two specific groups (uninjected and CRISPR)
751 against each other at every time point. Additionally, the mean percentage of EdU+ and Sox2+
752 cells in CRISPR and uninjected animals were compared at different time points using a 2-way
753 ANOVA with Sidak's test to compare every mean independently. Results are represented in
754 box plots or bar plots indicating the range between the 25th and 75th percentile, with all data
755 points shown. Single data points represent the average value of a given measurement per
756 animal, with error bars representing minimum to maximum values.

757

758 **Surgery for Spinal Cord Injury**

759 Before surgery, stage 50 tadpoles were placed in 0.1% MS222 in 0.1X MBS for
760 approximately 30 seconds until the reflex response to touch was absent. The animals were then
761 immobilized in a plasticine-coated petri dish and rinsed with transplantation solution (88 nM
762 NaCl, 1 mM KCl, 1 mM $MgSO_4$ x 7 H_2O, 5 mM HEPES, 3 mM $CaCl_2$, 100 units penicillin/ml,
763 0.1 mg/ml streptomycin), removing any excess solution. Dorsal skin and adjacent muscle
764 tissues from the mid-thoracic level were incised using fine forceps, exposing the spinal cord.
765 After removing a small portion of the meninges, a tungsten wire was inserted below the spinal
766 cord to lift it slightly, facilitating subsequent transection with a 25 gauge injection needle. For
767 sham injury, only the skin and muscle tissues were incised. Following surgery, the tadpoles

768 were placed in a transplantation buffer for 30 minutes before being transferred to 0.1X MBS
769 supplemented with antibiotics (400 mg/l penicillin, 400 mg/l streptomycin, and 25 mg/l
770 gentamicin) for the duration of the study. The animals were housed in individual wells in a six-
771 well plate in 0.1X MBS and supplemented with antibiotics, and the media was changed twice
772 daily for the first three days post-injury and once daily after that. Feeding the animals began
773 two days post-surgery, consisting of sera Micron Growth Food (Sera, 00720) in 0.1X MBS.
774 For pharmacological treatments, tadpoles were incubated post-surgery in DMSO, FIPI, and
775 S1P, using the aforementioned concentrations, and solutions were changed once daily for seven
776 days. Tadpoles were terminally anesthetized during the appropriate time points by prolonged
777 exposure (20 minutes) in 0.1% MS222. Following euthanasia, the tadpoles were rinsed twice
778 for 5 minutes in 1x PBS and fixed in 4% PFA overnight at 4°C.

779

780 **Swimming Recovery Test**

781 A quantitative recovery test was designed by recording and measuring vibration-induced
782 swimming to analyze the recovery of tadpoles following SCI. For this, tadpoles were placed in
783 a custom-made six-well plate attached to a 10 mm Pico Vibe vibration motor (Precision
784 Microdrives), connected via USB to a Mega 2560 MCU Board (Arduino). The vibration's
785 duration was programmed using Arduino's Integrated Development Environment. Tadpoles
786 were placed in the recording chamber for a 1-minute equilibration period and subsequently
787 recorded for 90 seconds, during which they were subjected to six 3-second stimulation pulses
788 at equal time intervals. After recording, total swimming distances were measured using
789 EthoVision XT video tracking software (Noldus) and analyzed in GraphPad Prism.

790
791

Acknowledgments

This study was funded by Science Foundation Ireland (SFI) and the European Regional Development Fund (ERDF) under grant number 13/RC/2073_P2. The authors acknowledge the use of the facilities of the Centre for Microscopy and Imaging at the University of Galway, Galway, Ireland, a facility that is co-funded by the Irish Government's Programme for Research in Third Level Institutions, Cycles 4 and 5, National Development Plan 2007–2013. During the course of this work M.E.A held a Hardiman fellowship from University of Galway and a Government of Ireland PhD Scholarship from the Irish Research Council (GOIPG/2018/500).

Competing Interest Statement: The authors have no competing interests.

Data and materials availability statement: All data are available in the main text or the supplementary materials.

References

Ahrens, K., & Schlosser, G. (2005). Tissues and signals involved in the induction of placodal Six1 expression in *Xenopus laevis*. *Dev.Biol., 288*(1), 40-59.

Alibardi, L. (2017). Biological and molecular differences between tail regeneration and limb scarring in lizard: an inspiring model addressing limb regeneration in amniotes. . *J. Exp. Zool. B (Mol. Dev. Evol.), 328*, 493-514.

Alunni, A., & Bally-Cuif, L. (2016). A comparative view of regenerative neurogenesis in vertebrates. *Development, 143*(5), 741-753. doi:10.1242/dev.122796

Aztekin, C., Hiscock, T. W., Marioni, J. C., Gurdon, J. B., Simons, B. D., & Jullien, J. (2019). Identification of a regeneration-organizing cell in the Xenopus tail. *Science, 364*(6441), 653-658. doi:10.1126/science.aav9996

Beattie, M. S., Bresnahan, J. C., & Lopate, G. (1990). Metamorphosis alters the response to spinal cord transection in Xenopus laevis frogs. *Journal of Neurobiology, 21*(7), 1108-1122. doi:10.1002/neu.480210714

Bhattacharya, D., Marfo, C. A., Li, D., Lane, M., & Khokha, M. K. (2015). CRISPR/Cas9: An inexpensive, efficient loss of function tool to screen human disease genes in Xenopus. *Developmental Biology, 408*(2), 196-204. doi:10.1016/j.ydbio.2015.11.003

Blitz, I. L., Biesinger, J., Xie, X., & Cho, K. W. (2013). Biallelic genome modification in F(0) Xenopus tropicalis embryos using the CRISPR/Cas system. *Genesis, 51*(12), 827-834.

Bock-Marquette, I., Shrivastava, S., Pipes, G. C., Thatcher, J. E., Blystone, A., Shelton, J. M., . . . DiMaio, J. M. (2009). Thymosin beta4 mediated PKC activation is essential to initiate the embryonic coronary developmental program and epicardial progenitor cell activation in adult mice in vivo. *Journal of Molecular and Cellular Cardiology, 46*(5), 728-738. doi:10.1016/j.yjmcc.2009.01.017

Brown, H. A., Thomas, P. G., & Lindsley, C. W. (2017). Targeting phospholipase D in cancer, infection and neurodegenerative disorders. *Nat Rev Drug Discov, 16*(5), 351-367. doi:10.1038/nrd.2016.252

Brudvig, J. J., & Weimer, J. M. (2015). X MARCKS the spot: myristoylated alanine-rich C kinase substrate in neuronal function and disease. *Frontiers in Cellular Neuroscience, 9*, 407. doi:10.3389/fncel.2015.00407

Carballo, E., Pitterle, D. M., Stumpo, D. J., Sperling, R. T., & Blackshear, P. J. (1999). Phagocytic and macropinocytic activity in MARCKS-deficient macrophages and fibroblasts. *American Journal of Physiology, 277*(1), C163-173. doi:10.1152/ajpcell.1999.277.1.C163

Carmichael, S. T., Archibeque, I., Luke, L., Nolan, T., Momiy, J., & Li, S. (2005). Growth-associated gene expression after stroke: evidence for a growth-promoting region in peri-infarct cortex. *Experimental Neurology, 193*(2), 291-311. doi:10.1016/j.expneurol.2005.01.004

Conant, D., Hsiau, T., Rossi, N., Oki, J., Maures, T., Waite, K., . . . Stoner, R. (2022). Inference of CRISPR Edits from Sanger Trace Data. *CRISPR J, 5*(1), 123-130. doi:10.1089/crispr.2021.0113

DeLay, B. D., Corkins, M. E., Hanania, H. L., Salanga, M., Deng, J. M., Sudou, N., . . . Miller, R. K. (2018). Tissue-Specific Gene Inactivation in Xenopus laevis: Knockout of lhx1 in the Kidney with CRISPR/Cas9. *Genetics, 208*(2), 673-686. doi:10.1534/genetics.117.300468

Edwards-Faret, G., Cebrian-Silla, A., Mendez-Olivos, E. E., Gonzalez-Pinto, K., Garcia-Verdugo, J. M., & Larrain, J. (2018). Cellular composition and organization of the spinal cord central canal during metamorphosis of the frog Xenopus laevis. *Journal of Comparative Neurology, 526*(10), 1712-1732. doi:10.1002/cne.24441

Edwards-Faret, G., Munoz, R., Mendez-Olivos, E. E., Lee-Liu, D., Tapia, V. S., & Larrain, J. (2017). Spinal cord regeneration in Xenopus laevis. *Nature Protocols, 12*(2), 372-389. doi:10.1038/nprot.2016.177

El Amri, M., Fitzgerald, U., & Schlosser, G. (2018). MARCKS and MARCKS-like proteins in development and regeneration. *Journal of Biomedical Science, 25*(1), 43. doi:10.1186/s12929-018-0445-1

Foster, D. A., & Xu, L. (2003). Phospholipase D in cell proliferation and cancer. *Molecular Cancer Research, 1*(11), 789-800.

Gaete, M., Munoz, R., Sanchez, N., Tampe, R., Moreno, M., Contreras, E. G., . . . Larrain, J. (2012). Spinal Cord Regeneration in Xenopus Tadpoles Proceeds through Activation of Sox2 Positive Cells. *Neural Dev, 7*(1), 13.

Gibbs, K. M., Chittur, S. V., & Szaro, B. G. (2011). Metamorphosis and the regenerative capacity of spinal cord axons in Xenopus laevis. *European Journal of Neuroscience, 33*(1), 9-25. doi:10.1111/j.1460-9568.2010.07477.x

Hartwig, J. H., Thelen, M., Rosen, A., Janmey, P. A., Nairn, A. C., & Aderem, A. (1992). MARCKS is an actin filament crosslinking protein regulated by protein kinase C and calcium-calmodulin. *Nature, 356*(6370), 618-622. doi:10.1038/356618a0

Iioka, H., Ueno, N., & Kinoshita, N. (2004). Essential role of MARCKS in cortical actin dynamics during gastrulation movements. *Journal of Cell Biology, 164*(2), 169-174. doi:10.1083/jcb.200310027

Kam, Y., & Exton, J. H. (2001). Phospholipase D activity is required for actin stress fiber formation in fibroblasts. *Molecular and Cellular Biology, 21*(12), 4055-4066. doi:10.1128/MCB.21.12.4055-4066.2001

Kanno, H., Ozawa, H., Sekiguchi, A., Yamaya, S., Tateda, S., Yahata, K., & Itoi, E. (2012). The role of mTOR signaling pathway in spinal cord injury. *Cell Cycle, 11*(17), 3175-3179. doi:10.4161/cc.21262

Kim, J., Blackshear, P. J., Johnson, J. D., & McLaughlin, S. (1994). Phosphorylation reverses the membrane association of peptides that correspond to the basic domains of MARCKS and neuromodulin. *Biophysical Journal, 67*(1), 227-237. doi:10.1016/S0006-3495(94)80473-4

Kshirsagar, A. (2020). *Integrated proteomic and systems biology approach to understanding injured spinal cord pathophysiology and repair.* National University of Ireland Galway, Galway, Ireland.

Laux, T., Fukami, K., Thelen, M., Golub, T., Frey, D., & Caroni, P. (2000). GAP43, MARCKS, and CAP23 modulate PI(4,5)P(2) at plasmalemmal rafts, and regulate cell cortex actin dynamics through a common mechanism. *Journal of Cell Biology, 149*(7), 1455-1472. doi:10.1083/jcb.149.7.1455

Lee-Liu, D., Edwards-Faret, G., Tapia, V. S., & Larrain, J. (2013). Spinal cord regeneration: lessons for mammals from non-mammalian vertebrates. *Genesis, 51*(8), 529-544. doi:10.1002/dvg.22406

Lee-Liu, D., Moreno, M., Almonacid, L. I., Tapia, V. S., Munoz, R., von Marees, J., . . . Larrain, J. (2014). Genome-wide expression profile of the response to spinal cord injury in Xenopus laevis reveals extensive differences between regenerative and non-regenerative stages. *Neural Dev, 9*(1), 12. doi:10.1186/1749-8104-9-12

Lee, E., Tardi, P. G., Man, R. Y., & Choy, P. C. (1995). The modulation of phosphatidylinositol biosynthesis in hamster hearts by methyl lidocaine. *Biochemical Journal, 309 (Pt 3)*(Pt 3), 871-876. doi:10.1042/bj3090871

Liu, W. S., & Heckman, C. A. (1998). The sevenfold way of PKC regulation. *Cellular Signalling, 10*(8), 529-542. doi:10.1016/s0898-6568(98)00012-6

Lu, S., Yang, L., Jiang, H., Chen, J., Yu, G., Chen, Z., . . . He, S. (2019). Bichirs employ similar genetic pathways for limb regeneration as are used in lungfish and salamanders. *Gene, 690*, 68-74. doi:10.1016/j.gene.2018.12.031

McLaughlin, S., & Aderem, A. (1995). The myristoyl-electrostatic switch: a modulator of reversible protein-membrane interactions. *Trends in Biochemical Sciences, 20*(7), 272-276. doi:10.1016/s0968-0004(00)89042-8

McLaughlin, S., Wang, J., Gambhir, A., & Murray, D. (2002). PIP(2) and proteins: interactions, organization, and information flow. *Annual Review of Biophysics and Biomolecular Structure, 31*, 151-175. doi:10.1146/annurev.biophys.31.082901.134259

McNamara, R. K., Jiang, Y., Streit, W. J., & Lenox, R. H. (2000). Facial motor neuron regeneration induces a unique spatial and temporal pattern of myristoylated alanine-rich C kinase substrate expression. *Neuroscience, 97*(3), 581-589. doi:10.1016/s0306-4522(00)00039-7

Meacci, E., Nuti, F., Catarzi, S., Vasta, V., Donati, C., Bourgoin, S., . . . Vaughan, M. (2003). Activation of phospholipase D by bradykinin and sphingosine 1-phosphate in A549 human lung adenocarcinoma cells via different GTP-binding proteins and protein kinase C delta signaling pathways. *Biochemistry, 42*(2), 284-292. doi:10.1021/bi026350a

Monovich, L., Mugrage, B., Quadros, E., Toscano, K., Tommasi, R., LaVoie, S., . . . Steed, P. (2007). Optimization of halopemide for phospholipase D2 inhibition. *Bioorganic and Medicinal Chemistry Letters, 17*(8), 2310-2311. doi:10.1016/j.bmcl.2007.01.059

Morash, S. C., Byers, D. M., & Cook, H. W. (2000). Activation of phospholipase D by PKC and GTPgammaS in human neuroblastoma cells overexpressing MARCKS. *Biochimica et Biophysica Acta, 1487*(2-3), 177-189. doi:10.1016/s1388-1981(00)00094-9

Morash, S. C., Rose, S. D., Byers, D. M., Ridgway, N. D., & Cook, H. W. (1998). Overexpression of myristoylated alanine-rich C-kinase substrate enhances activation of phospholipase D by protein kinase C in SK-N-MC human neuroblastoma cells. *Biochemical Journal, 332 (Pt 2)*(Pt 2), 321-327. doi:10.1042/bj3320321

Munoz, R., Edwards-Faret, G., Moreno, M., Zuniga, N., Cline, H., & Larrain, J. (2015). Regeneration of Xenopus laevis spinal cord requires Sox2/3 expressing cells. *Developmental Biology, 408*(2), 229-243. doi:10.1016/j.ydbio.2015.03.009

Nieuwkoop, P. D., & Faber, J. (1967). *Normal table of Xenopus laevis (Daudin)*. Amsterdam: North-Holland.

Nogueira, A. F., Costa, C. M., Lorena, J., Moreira, R. N., Frota-Lima, G. N., Furtado, C., . . . Schneider, I. (2016). Tetrapod limb and sarcopterygian fin regeneration share a core genetic programme. *Nat Commun, 7*, 13364. doi:10.1038/ncomms13364

Penailillo, J., Palacios, M., Mounieres, C., Munoz, R., Slater, P. G., De Domenico, E., . . . Larrain, J. (2021). Analysis of the early response to spinal cord injury identified a key role for mTORC1 signaling in the activation of neural stem progenitor cells. *NPJ Regen Med, 6*(1), 68. doi:10.1038/s41536-021-00179-3

Rodemer, W., Hu, J., Selzer, M. E., & Shifman, M. I. (2020). Heterogeneity in the regenerative abilities of central nervous system axons within species: why do some neurons regenerate better than others? *Neural Regen Res, 15*(6), 996-1005. doi:10.4103/1673-5374.270298

Schlosser, G., & Ahrens, K. (2004). Molecular anatomy of placode development in *Xenopus laevis*. *Dev Biol., 271*(2), 439-466.

Semenas, J., Hedblom, A., Miftakhova, R. R., Sarwar, M., Larsson, R., Shcherbina, L., . . . Persson, J. L. (2014). The role of PI3K/AKT-related PIP5K1alpha and the discovery of its selective inhibitor for treatment of advanced prostate cancer. *Proceedings of the*

National Academy of Sciences of the United States of America, 111(35), E3689-3698. doi:10.1073/pnas.1405801111

Session, A. M., Uno, Y., Kwon, T., Chapman, J. A., Toyoda, A., Takahashi, S., . . . Rokhsar, D. S. (2016). Genome evolution in the allotetraploid frog *Xenopus laevis*. *Nature, 538*(7625), 336-343. doi:10.1038/nature19840

Shen, G. X. (2003). Selective protein kinase C inhibitors and their applications. *Current Drug Targets: Cardiovascular & Haematological Disorders, 3*(4), 301-307. doi:10.2174/1568006033481375

Sive, H. L., Grainger, R. M., & Harland, R. M. (2000). *Early development of Xenopus laevis* Cold Spring Harbor, New York: Cold Spring Harbor Laboratory Press.

Sousounis, K., Bhavsar, R., Looso, M., Kruger, M., Beebe, J., Braun, T., & Tsonis, P. A. (2014). Molecular signatures that correlate with induction of lens regeneration in newts: lessons from proteomic analysis. *Hum Genomics, 8*(1), 22. doi:10.1186/s40246-014-0022-y

Stumpo, D. J., Eddy, R. L., Jr., Haley, L. L., Sait, S., Shows, T. B., Lai, W. S., . . . Blackshear, P. J. (1998). Promoter sequence, expression, and fine chromosomal mapping of the human gene (MLP) encoding the MARCKS-like protein: identification of neighboring and linked polymorphic loci for MLP and MACS and use in the evaluation of human neural tube defects. *Genomics, 49*(2), 253-264. doi:10.1006/geno.1998.5247

Su, W., Yeku, O., Olepu, S., Genna, A., Park, J. S., Ren, H., . . . Frohman, M. A. (2009). 5-Fluoro-2-indolyl des-chlorohalopemide (FIPI), a phospholipase D pharmacological inhibitor that alters cell spreading and inhibits chemotaxis. *Molecular Pharmacology, 75*(3), 437-446. doi:10.1124/mol.108.053298

Sugiura, T., Wang, H., Barsacchi, R., Simon, A., & Tanaka, E. M. (2016). MARCKS-like protein is an initiating molecule in axolotl appendage regeneration. *Nature, 531*(7593), 237-240. doi:10.1038/nature16974

Sun, Y., & Chen, J. (2008). mTOR signaling: PLD takes center stage. *Cell Cycle, 7*(20), 3118-3123. doi:10.4161/cc.7.20.6881

Sundaram, M., Cook, H. W., & Byers, D. M. (2004). The MARCKS family of phospholipid binding proteins: regulation of phospholipase D and other cellular components. *Biochemistry and Cell Biology, 82*(1), 191-200. doi:10.1139/o03-087

Szpara, M. L., Vranizan, K., Tai, Y. C., Goodman, C. S., Speed, T. P., & Ngai, J. (2007). Analysis of gene expression during neurite outgrowth and regeneration. *BMC Neuroscience, 8*, 100. doi:10.1186/1471-2202-8-100

Trovo, L., Ahmed, T., Callaerts-Vegh, Z., Buzzi, A., Bagni, C., Chuah, M., . . . Dotti, C. G. (2013). Low hippocampal PI(4,5)P(2) contributes to reduced cognition in old mice as a result of loss of MARCKS. *Nature Neuroscience, 16*(4), 449-455. doi:10.1038/nn.3342

Veldman, M. B., Bemben, M. A., Thompson, R. C., & Goldman, D. (2007). Gene expression analysis of zebrafish retinal ganglion cells during optic nerve regeneration identifies KLF6a and KLF7a as important regulators of axon regeneration. *Developmental Biology, 312*(2), 596-612. doi:10.1016/j.ydbio.2007.09.019

Wallingford, J. B., Rowning, B. A., Vogeli, K. M., Rothbächer, U., Fraser, S. E., & Harland, R. M. (2000). Dishevelled controls cell polarity during Xenopus gastrulation. *Nature, 405*(6782), 81-85.

Wohnsland, F., Schmitz, A. A., Steinmetz, M. O., Aebi, U., & Vergeres, G. (2000). Interaction between actin and the effector peptide of MARCKS-related protein. Identification of functional amino acid segments. *Journal of Biological Chemistry, 275*(27), 20873-20879. doi:10.1074/jbc.M910298199

Xu, X. H., Deng, C. Y., Liu, Y., He, M., Peng, J., Wang, T., . . . Luo, Z. G. (2014). MARCKS regulates membrane targeting of Rab10 vesicles to promote axon development. *Cell Research, 24*(5), 576-594. doi:10.1038/cr.2014.33

Yarmola, E. G., Edison, A. S., Lenox, R. H., & Bubb, M. R. (2001). Actin filament cross-linking by MARCKS: characterization of two actin-binding sites within the phosphorylation site domain. *Journal of Biological Chemistry, 276*(25), 22351-22358. doi:10.1074/jbc.M101457200

Zhang, Y., Huang, P., Du, G., Kanaho, Y., Frohman, M. A., & Tsirka, S. E. (2004). Increased expression of two phospholipase D isoforms during experimentally induced hippocampal mossy fiber outgrowth. *Glia, 46*(1), 74-83. doi:10.1002/glia.10322

Zhao, H., Cao, Y., & Grunz, H. (2001). Isolation and characterization of a Xenopus gene (XMLP) encoding a MARCKS-like protein. *International Journal of Developmental Biology, 45*(7), 817-826.

Zhou, X., & Li, J. (2000). Macrophage-enriched myristoylated alanine-rich C kinase substrate and its phosphorylation is required for the phorbol ester-stimulated diffusion of beta 2 integrin molecules. *Journal of Biological Chemistry, 275*(26), 20217-20222. doi:10.1074/jbc.M909129199

Figures

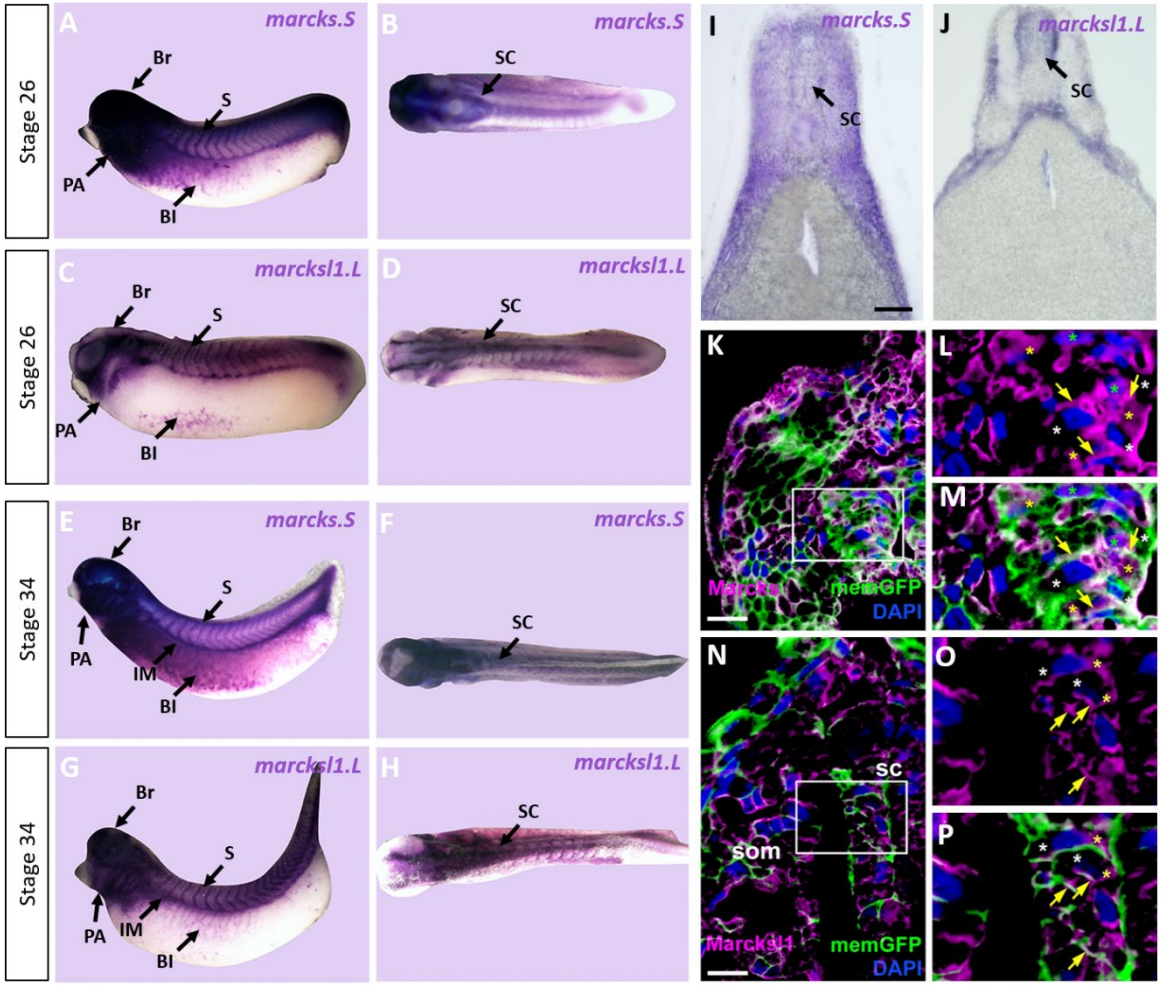

Fig. 1: Expression of Marcks and Marcksl1 in the *Xenopus* spinal cord.
A-H: Expression of *marcks.S* (A, B, E, F) and *marcksl1.L* (C, D, G, H) as revealed by whole-mount in situ hybridization in stage 26 (A-D) and 34 (E-H) *Xenopus* embryos in lateral (A,C,E,G) and dorsal (B,D,F,H) views (anterior is to the left). Expression in the spinal cord (SC), brain (Br), somites (S), intermediate mesoderm (IM), blood islands (Bl), and pharyngeal arches (PA) is indicated. I, J: Transverse sections showing expression of *marcks.S* (I) and *marcksl1.L* (J) in the spinal cord at stage 34. K-P: Immunostaining for Marcks (K-M) and Marcksl1 (N-P) protein in confocal images of transverse sections through stage 26 embryos after *memGFP* mRNA injection. White boxed areas in (K) and (N) are shown at a higher magnification in (L, M) and (N, O), respectively. Yellow asterisks indicate the expression of Marcks in the cytoplasm; green asterisks indicate expression in nuclei; white asterisks show the absence of expression in the cytoplasm; yellow arrows show expression in the membrane. Abbreviations: sc, spinal cord; som, somites. Scale bar in I = 50 µm (for I, J). Scale bar in K and N = 20 µm.

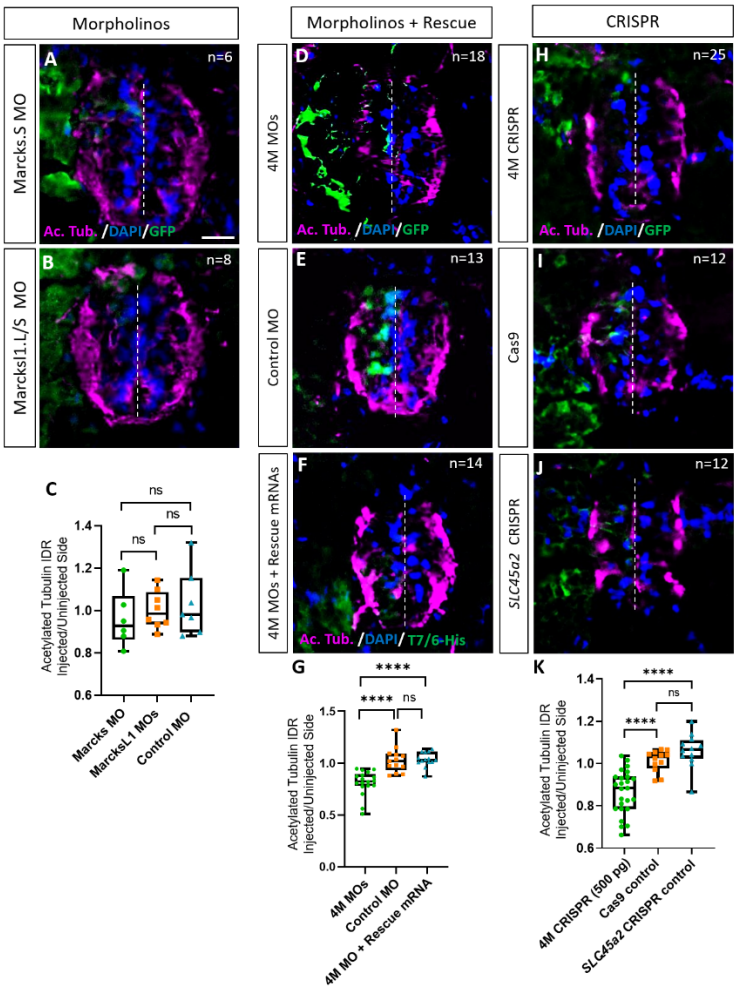

Fig. 2: Marcks and Marcksl1 are required for neurite outgrowth during *Xenopus* spinal cord development.

A-C: Evaluation of neurite outgrowth after individual morpholino (MO) knockdown of Marcks or Marcksl1 in stage 34-36 developing spinal cords. One blastomere of 4-8 cell stage embryos was injected with either 9 ng of marcks MOs (A, C), 9 ng of marcksl1.L and marcksl1.S MOs each (B, C), or 9 ng of control MO (C). All injections contained 125 pg of *myc-GFP* mRNA to identify the injected side. D-J: Evaluation of neurite outgrowth after loss of function of all four homeologs (*marcks.S, marcks.L*, *marcksl1.S* and *marcksl1.L)* by MO knockdown (4M MO) or CRISPR knockout (4M CRISPR). One blastomere of 4-8 cell stage embryos was co-injected with 9 ng of each MO (marcks.S, marcksl1.L, and marcksl1.S MO) (D, G); 27 ng standard control MO (E, G); 9 ng of each MO plus 300 pg of mutated chicken *marcks* and 350 pg of mutated *X. tropicalis marcksl1* rescue mRNA constructs encoding T7 and 6-His tags (F, G); 500 pg of each single-guide RNA (*marcks.L/S* and *marcksl1.L/S* sgRNA) with 1 ng Cas9 protein (H, K); 1 ng Cas9 protein (I, K); or *slc45a2* sgRNA and 1 ng Cas9 protein (J, K). All injections contained 125 pg of myc-GFP mRNA to identify the injected side. Injected (left) and uninjected (right) spinal cord sides (separated by the dashed line) were compared in transverse sections immunostained for acetylated tubulin (A, B, D-F, H-J) and for GFP, T7, and 6-His to determine the injected side. Immunostaining for acetylated tubulin was quantified (G, K) by determining the integrated density ratio (IDR) of staining in injected to uninjected sides. Significance was determined using an ordinary one-way ANOVA with Tukey's multiple comparisons test. NS, not significant; ****P<0.0001. Error bars represent minimum to maximum values showing all points with a line at the median. n refers to the number of animals analyzed. Scale bar in A = 25 µm (for all panels).

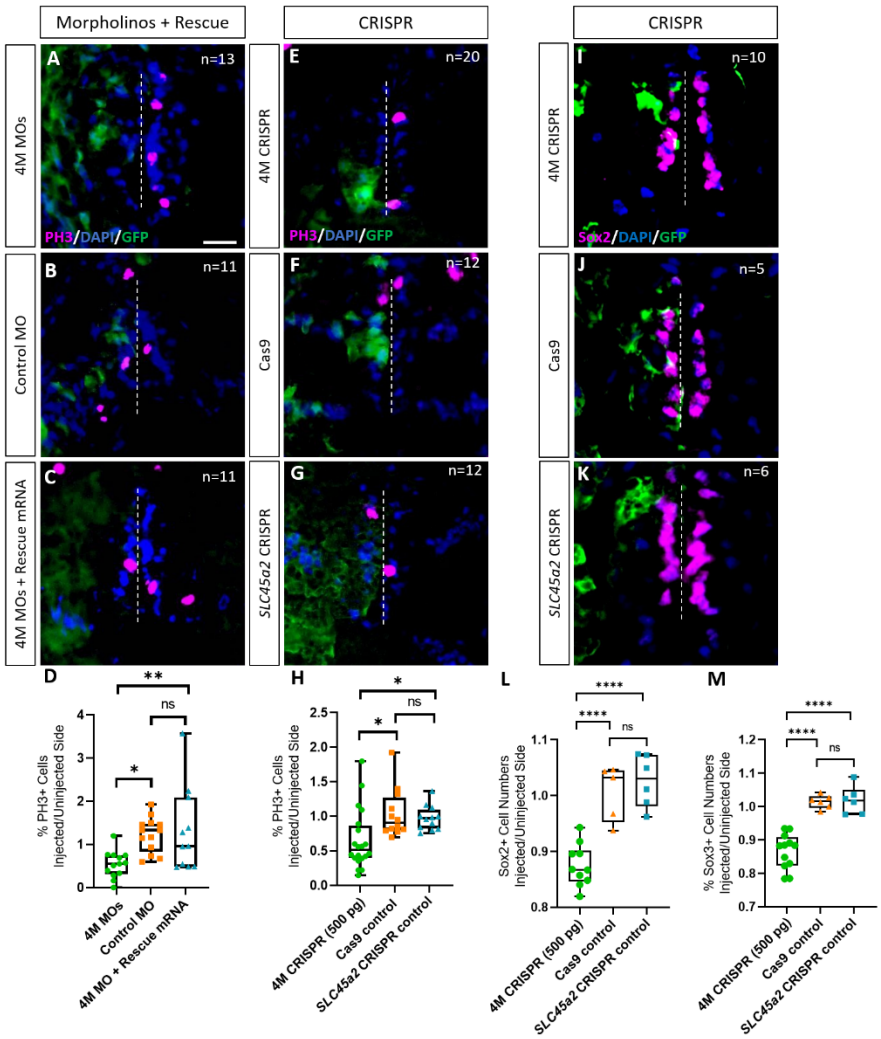

Fig. 3: **Marcks and Marcksl1 are required for the proliferation of neuro-glial progenitors during *Xenopus* spinal cord development.**

Evaluation of mitotic activity (A-H) or number of neuro-glial progenitors (I-M) after loss of function of all four homeologs (*marcks.S, marcks.L*, *marcksl1.S* and *marcksl1.L)* by MO knockdown (4M MO) or CRISPR knockout (4M CRISPR). One blastomere of 4-8 cell stage embryos was co-injected with 9 ng of each MO (marcks.S, marcksl1.L, and marcksl1.S MO) (A, D); 27 ng standard control MO (B, D); 9ng of each MO plus 300 pg of mutated chicken *marcks* and 350 pg of mutated *X. tropicalis marcksl1* rescue mRNA constructs encoding T7 and 6-His tags (C, D); 500 pg of each single-guide RNA (*marcks.L/S* and *marcksl1.L/S* sgRNA) with 1 ng Cas9 protein (E, H, I); 1 ng Cas9 protein (F, H, J); or *slc45a2* sgRNA and 1 ng Cas9 protein (G, H, K). All injections contained 125 pg of *myc-GFP* mRNA to identify the injected side. Injected (left) and uninjected (right) spinal cord sides (separated by the dashed line) were compared in transverse sections of stage 34-36 embryos immunostained for phospho-histone 3 (PH3) (A-C, E-G) or Sox2 (I-K) and for GFP, T7, and 6-His to determine the injected side. Mitotic or neuro-glial progenitor cells were quantified by determining the ratio of the percentage of PH3+ cells (D) and the numbers of Sox2+ (L) or Sox3+ (M) cells on injected and uninjected sides. Significance was determined using an ordinary one-way ANOVA with Tukey's multiple comparisons test. NS, not significant; *P<0.05; **P≤0.01; ****P<0.0001. Error bars represent minimum to maximum values showing all points with the line at median. n refers to the number of animals analyzed. Scale bar in A = 25 µm (for all panels).

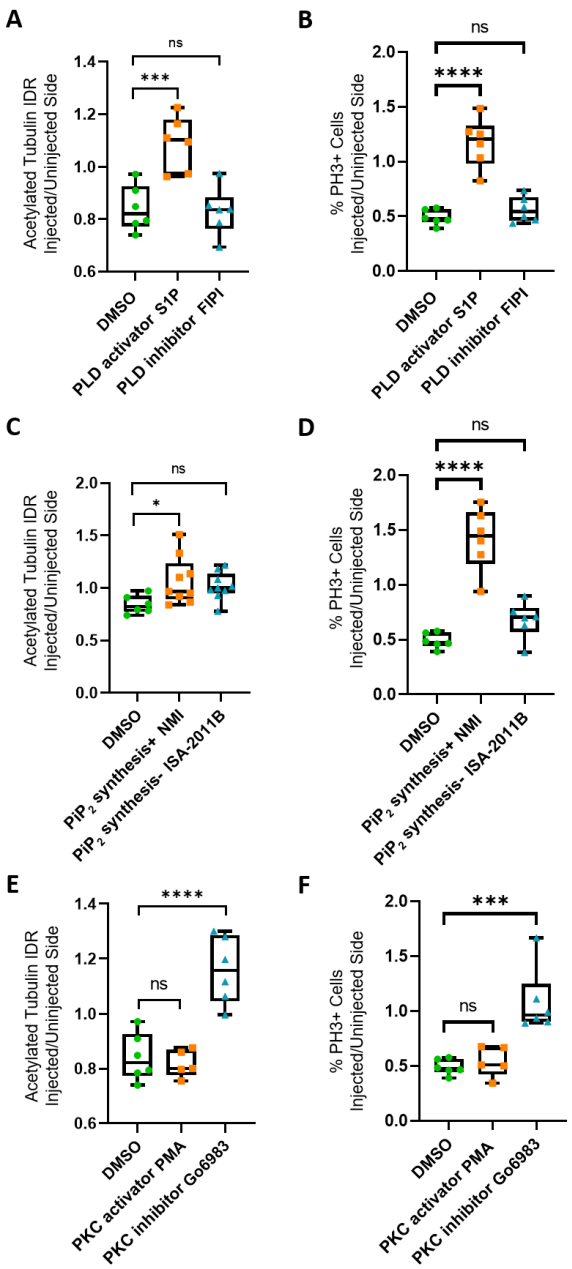

Fig. 4: Rescue of Marcks and Marcksl1 knockout phenotype by activating Phospholipase D (PLD) and other signaling pathways.

One blastomere of 4-8 cell stage embryos was co-injected with 500 pg of each single-guide RNA (*marcks.L/S* and *marcksl1.L/S* sgRNA), 1 ng Cas9 protein and 125 pg myc-GFP mRNA to knockout all four homeologs (4M CRISPR). Embryos were then incubated in compounds modulating PLD signaling (A, B), PIP_2 synthesis (C, D), or protein kinase C (PKC) activity (E, F) and analyzed for neurite outgrowth (integrated density ratio or IDR of acetylated tubulin on injected versus uninjected sides) and mitotic activity (ratio of the proportion of PH3+ cells on injected versus uninjected sides). Significance was determined using an ordinary one-way ANOVA with Dunnett's multiple comparisons test. NS, not significant; *P<0.05; **P≤0.01; ***P<0.001; ****P<0.0001. Error bars represent minimum to maximum values showing all points with the line at the median. n refers to the number of animals analyzed. Neurite outgrowth and mitotic activity was significantly increased (rescued) in the spinal cord of 4M-CRISPR embryos by PLD activators, enhancers of PIP_2 synthesis, and PKC inhibitors. In contrast, PLD inhibitors, inhibitors of PIP_2 synthesis, and PKC activators had no effect.

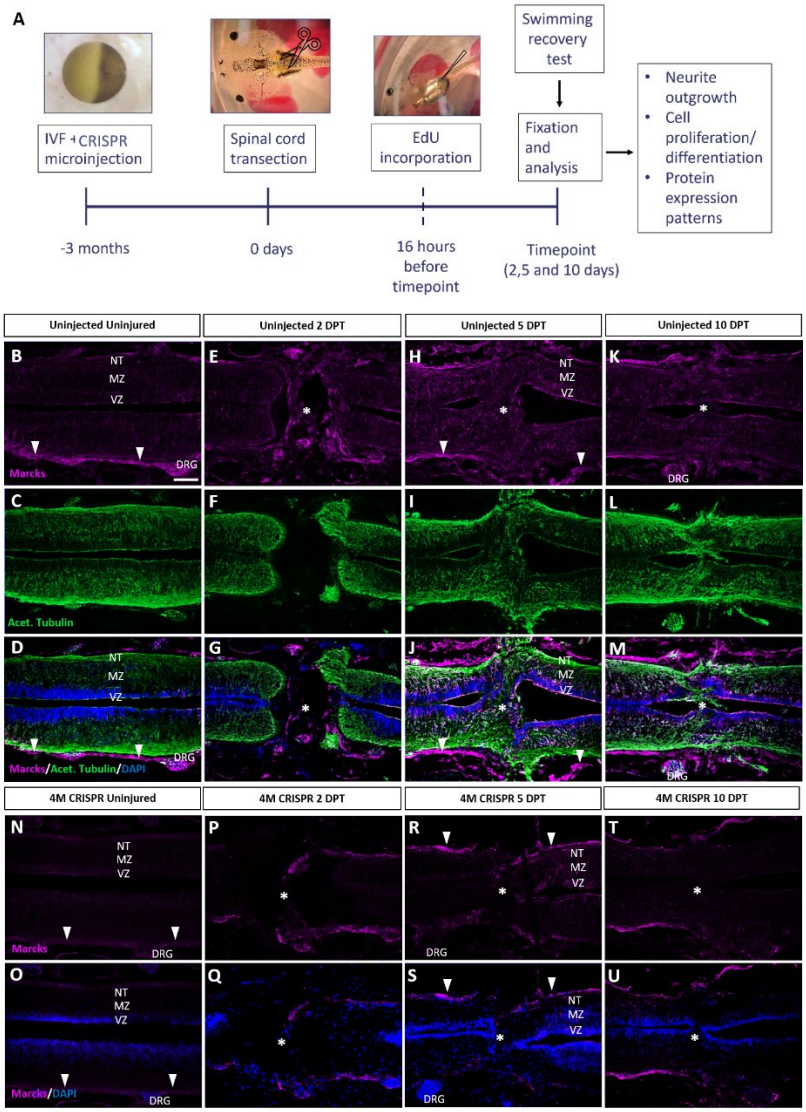

Fig. 5: Upregulation of Marcks proteins after spinal cord transection is abolished after knockout of Marcks and Marcksl1.

A: Experimental flow of the spinal cord injury study. 1-cell stage embryos were injected with CRISPR constructs targeting all homeologs of Marcks and Marcksl1. After approximately three months, the spinal cords of uninjected and CRISPR tadpoles (stage 50) were transected. Tadpoles underwent a swimming recovery test at 2-, 5-, and 10-days post transection (DPT). They were analyzed by immunostaining for regenerative outcomes, including neurite outgrowth and injury gap closure, cell proliferation (after prior EdU injection), and neuro-glial progenitor markers. B-M: Immunostaining for Marcks in horizontal sections of uninjected stage 50 tadpoles without injury (B-D) or at 2 DPT (E-G), 5 DPT (H-J), and 10 DPT (K-M). Before the injury, Marcks immunostaining was weakly detected in the ventricular zone (VZ), mantle zone (MZ), and the neurite tracts (NT) of the marginal zone of the spinal cord as well as in the dorsal root ganglia (DRG) and meninges (white arrowheads). After spinal cord transection, it was upregulated in all layers of the spinal cord cells surrounding the injury gap and in cells infiltrating the injury site (white asterisks). Scale bar = 50 µm. N=6 tadpoles per condition. N-U: Immunostaining for Marcks in horizontal sections of 4M CRISPR-injected stage 50 tadpoles without injury (N, O) or at 2 DPT (P, Q), 5 DPT (R, S), and 10 DPT (T, U). Barely any Marcks immunostaining is detectable at any time point. N=6 tadpoles per condition. Scale bar in B = 50 µm (for all panels).

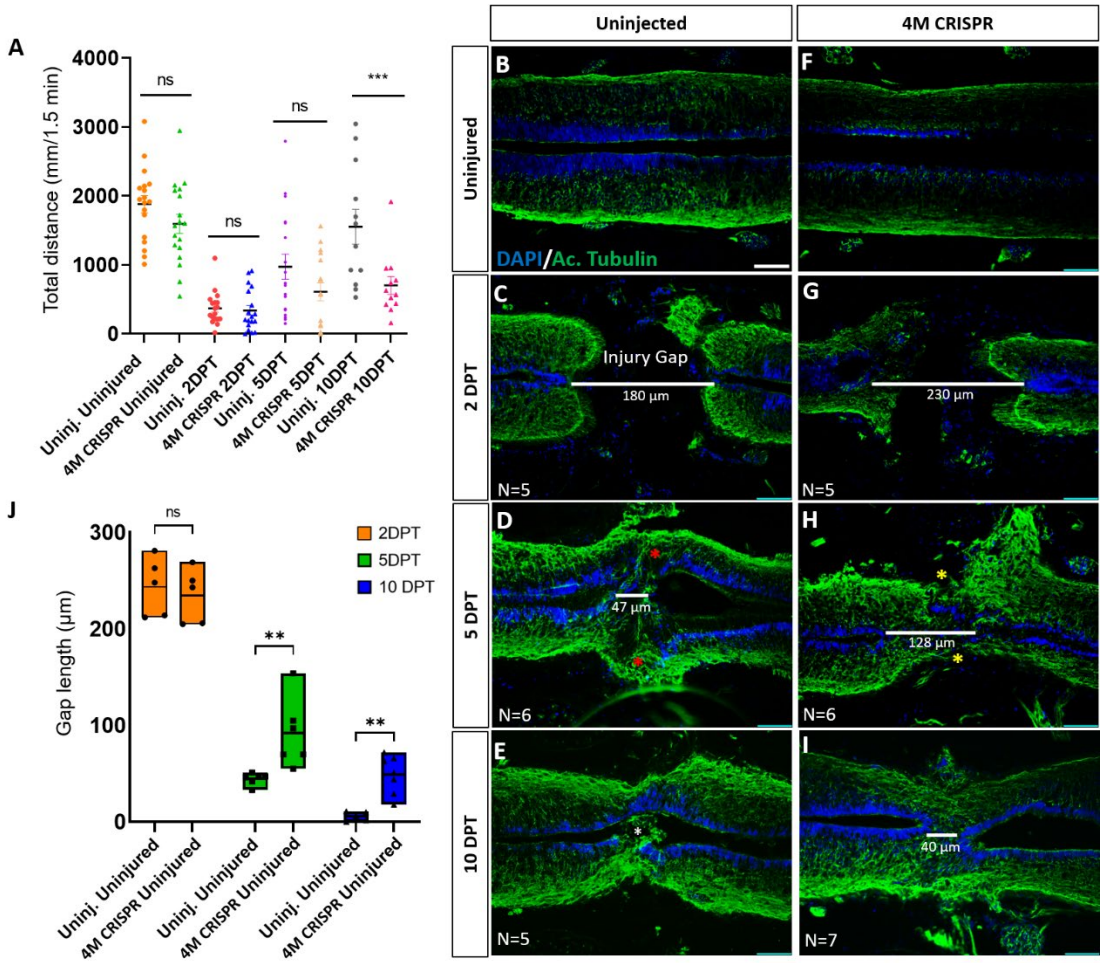

Fig. 6: Functional recovery and injury gap closure after spinal cord transection are compromised after knockout of Marcks and Marcksl1.

A: Swimming recovery test in stage 50 tadpoles after spinal cord injury. The graph shows the total swimming distance in uninjected and 4M CRISPR-injected animals before the injury and at 2-, 5-, and 10- DPT. The y-axis indicates the distance traveled by the tadpoles in millimeters for 90 seconds. Significance was determined using an ordinary one-way ANOVA with an uncorrected Fisher's least significant difference (LSD) test for multiple comparisons. NS, not significant; ***P<0.001. All data points are shown with the line at mean with SEM. Error bars represent the standard error of the mean. B-J: Comparison of injury gap closure between uninjected and 4M CRISPR-injected stage 50 tadpoles after spinal cord transection. Immunostaining for acetylated tubulin marking axonal tracts with DAPI marking nuclei in horizontal sections of the spinal cord (B-I) and quantifying injury gap length (J). Gap length was measured as the distance between the ventricular zones of rostral and caudal spinal cord stumps, as indicated by the white lines. At 2 DPT, an injury gap is visible in uninjected (B) and 4M CRISPR-injected (F) tadpoles. Axonal bridges connecting the rostral and caudal injury gap in the uninjected tadpoles at 5 DPT (red asterisks) are absent in the 4M CRISPR animals (yellow asterisks). The central canal in uninjected tadpoles becomes continuous at 10 DPT (E), in contrast to the 4M CRISPR-injected tadpoles (I). Significance was determined using a 2-way ANOVA with uncorrected Fisher's LSD of multiple comparisons. NS, not significant; **P≤0.01. All data points are shown with the line at the mean. Scale bar in B = 50 µm (for B-H).

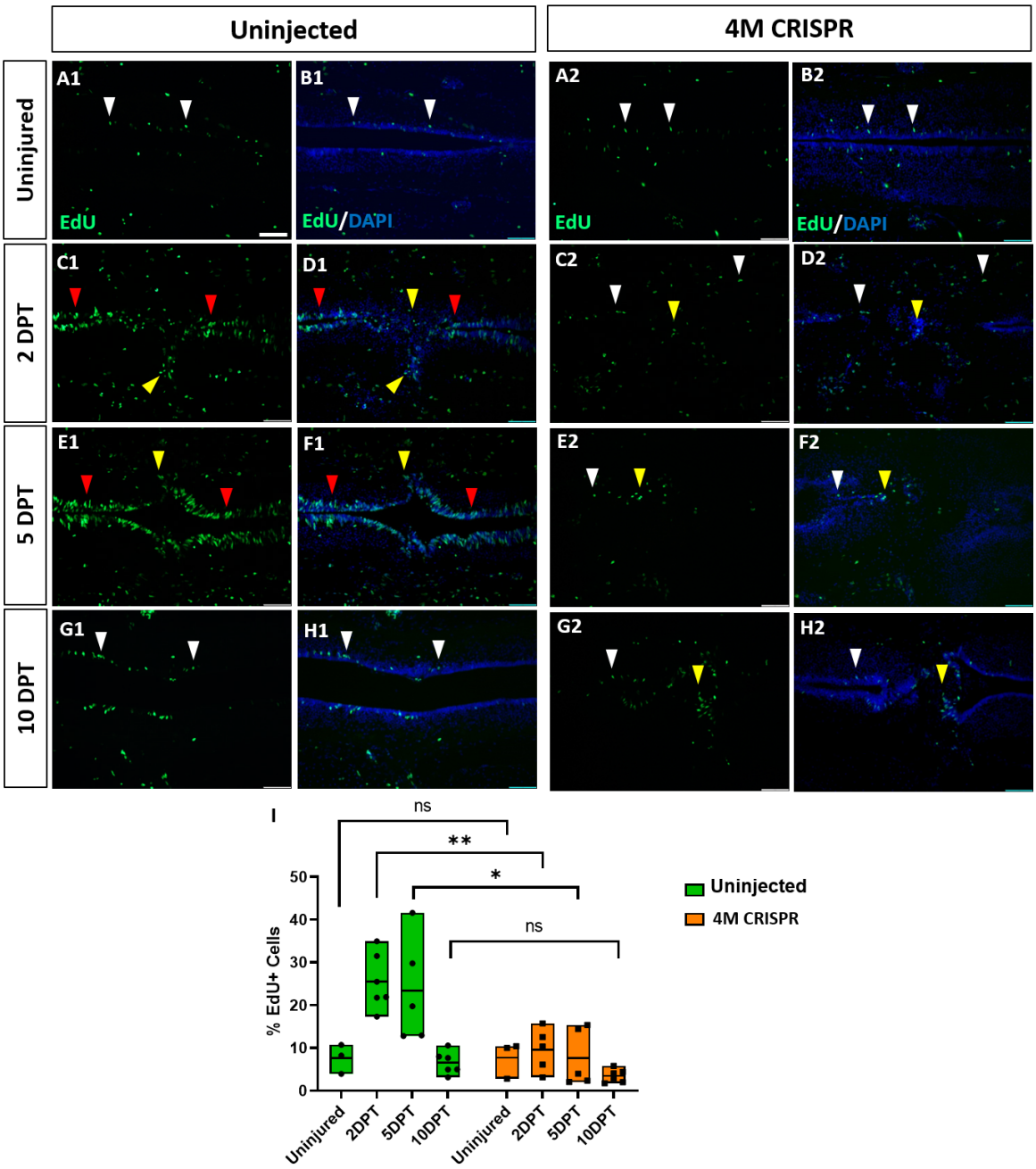

Fig. 7: Upregulation of cell proliferation after spinal cord transection is compromised after knockout of Marcks and Marcksl1.

A-H: Evaluation of EdU+ proliferative cells at 2-, 5-, and 10-DPT in horizontal sections of uninjected (A1-H1) and 4M CRISPR-injected tadpoles (A2-H2) at stage 50 (A-H) and quantification of the average proportion of EdU+ cells in a defined window of the spinal cord adjacent to the injury site (I). White and red arrowheads indicate preinjury and elevated levels of EdU+ cells in the ventricular zone, respectively. Yellow arrowheads indicate EdU+ cells in and adjacent to the injury gap. Note the increase in EdU+ cells at 2 DPT and 5 DPT in uninjected (C1-F1, I) but not 4M CRISPR-injected (C2-F2, I) tadpoles. Significance was determined using a 2-way ANOVA with Sidak's multiple comparisons test. NS, not significant; **P≤0.01; ***P<0.001. All data points are shown with the line at mean. Scale bar in A1 = 50 µm (for all panels).

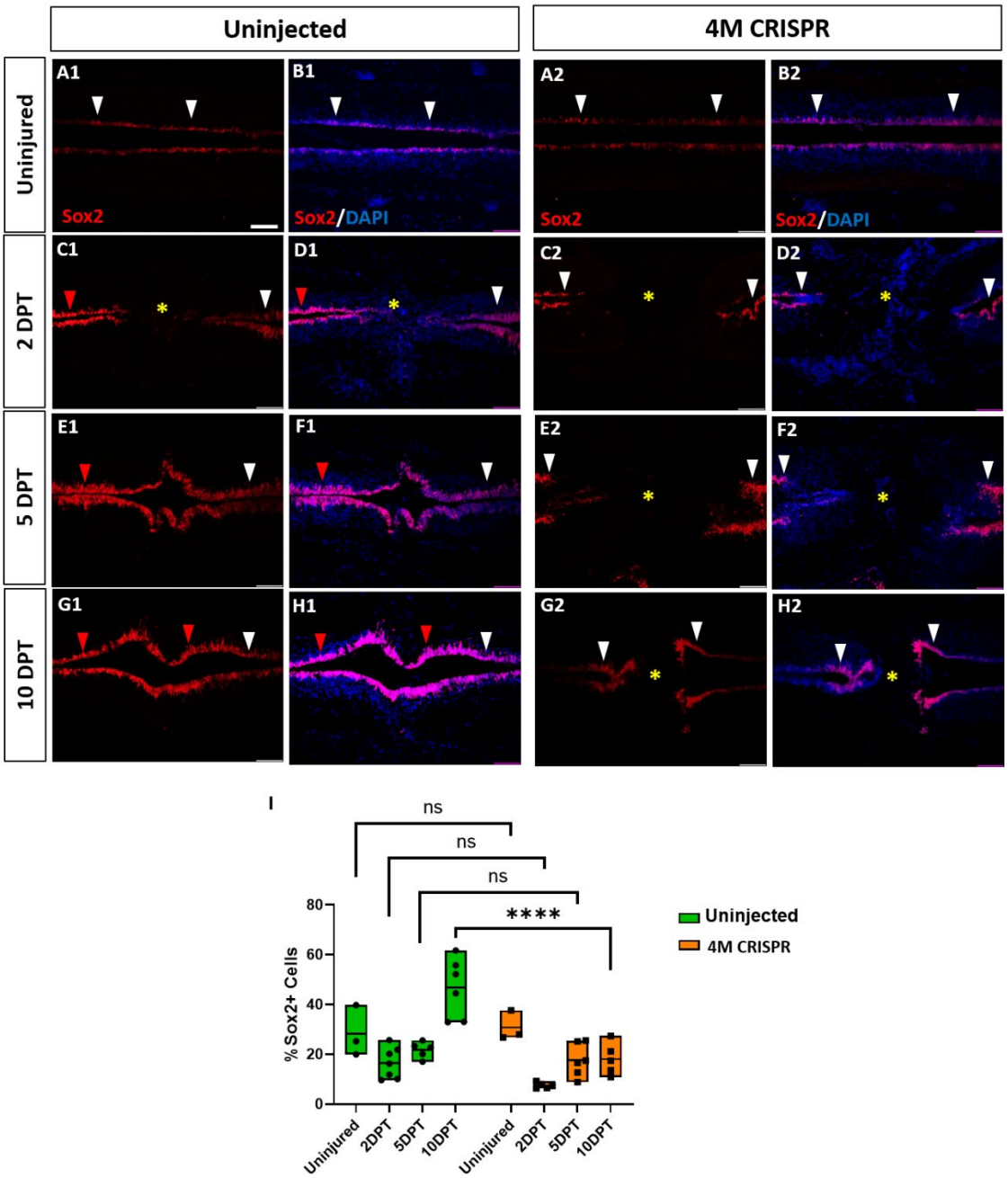

Fig. 8: Expansion of Sox2+ neuro-glial progenitors after spinal cord transection is compromised after knockout of Marcks and Marcksl1.

A-H: Evaluation of Sox2+ neuro-glial progenitors at 2-, 5-, and 10-DPT in horizontal sections of uninjected (A1-H1) and 4M CRISPR-injected tadpoles (A2-H2) at stage 50 (A-H) and quantification of the average proportion of Sox2+ cells in a defined window of the spinal cord adjacent to the injury site (I). White and red arrowheads indicate preinjury and elevated levels of Sox2+ cells in the ventricular zone, respectively. A yellow asterisk indicates the absence of Sox2+ cells in and adjacent to the injury gap. Note the increase in Sox2+ cells in the spinal cord rostral to the injury gap at 2 DPT (C1, D1) and the increase in the proportion of Sox2+ cells at 10 DPT (G1, H1, I) in uninjected but not 4M CRISPR-injected tadpoles (C2, D2, G2, H2, I). Significance was determined using a 2-way ANOVA with Sidak's multiple comparisons test. NS, not significant; **P≤0.01; ***P<0.001. All data points are shown with the line at mean. Scale bar in A1 = 50 µm (for all panels).

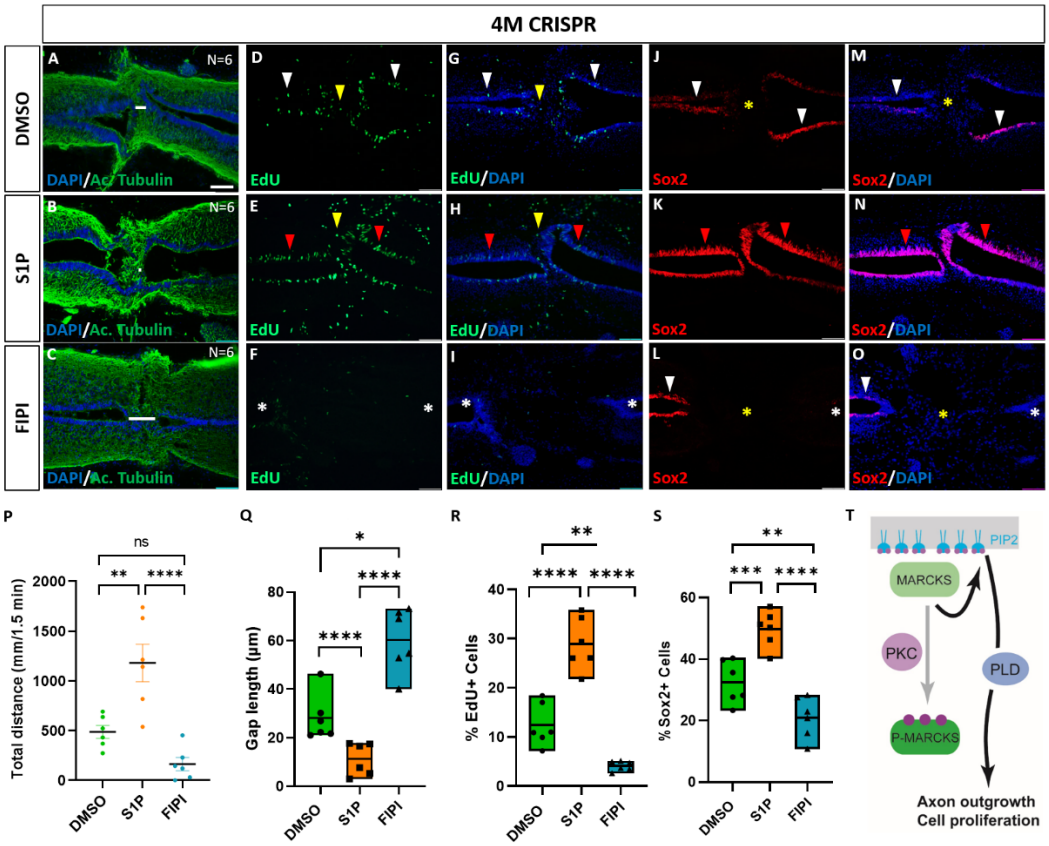

Fig. 9: Activation of Phospholipase D (PLD) signaling rescues deficiencies of spinal cord regeneration in 4M CRISPR-injected tadpoles.

A-O: Horizontal sections of 4M CRISPR-injected tadpoles at stage 50 exposed to DMSO only (controls; A, D, G, J, M) or to PLD activator S1P (B, E, H, K, N) or PLD inhibitor FIPI (C, F, J, L, O) for 7 DPT and analyzed for injury gap closure (A-C); the proportion of proliferative EdU+ cells (D-I) and proportion of Sox2+ neuro-glial progenitors (J-O). Immunostaining for acetylated tubulin and nuclear DAPI staining was used to visualize injury gap closure (A-C). Gap length was measured as the distance between the ventricular zones of rostral and caudal spinal cord stumps, as indicated by the white lines. White and red arrowheads indicate preinjury and elevated levels of EdU+ or Sox2+ cells in the ventricular zone, respectively. Yellow arrowheads indicate EdU+ cells in and adjacent to the injury gap. White asterisks indicate reduced levels of EdU+ or Sox2+ cells in the ventricular zone. A yellow asterisk indicates the absence of Sox2+ cells in and adjacent to the injury gap. P-S: Quantification of effects of pharmacological treatments in 4M CRISPR-injected tadpoles at 7 DPT on swimming recovery (P), injury gap closure (Q), proportion of proliferative EdU+ cells (R), and proportion of Sox2+ neuro-glial progenitors (S). Note that the PLD activator S1P significantly enhances swimming recovery, injury gap closure, and proportions of proliferating cells (EdU+) and neuro-glial progenitors (Sox2+) after spinal cord transection in 4M CRISPR tadpoles compared to DMSO-treated controls. At the same time, the PLD inhibitor FIPI significantly reduces injury gap closure and proportions of proliferating cells (EdU+) and neuro-glial progenitors (Sox2+). Significance was determined using an ordinary one-way ANOVA with uncorrected Fisher's LSD for multiple comparisons. N=6 animals per condition. NS, not significant; *P<0.05; **P≤0.01; ***P<0.001; ****P<0.0001. All data points are shown with the line at mean. Error bars in (P) represent the standard error of the mean. Scale bar in A = 50 µm (for all panels). T: Model proposing that unphosphorylated, membrane-bound Marcks and Marcksl1 proteins promote axon outgrowth and proliferation during spinal cord development and regeneration in a PIP_2 and PLD-dependent manner.

1212

1213

1214 **Table 1** Primary Antibodies

Antigen	Company, Product Code	Reactivity	Dilution
Acetylated Tubulin	Sigma, T6793	Mouse Monoclonal	1:1000
Phospho-Histone H3 (PH3)	Merck, 06-570	Rabbit Polyclonal	1:200
GFP	Abcam, ab290	Rabbit Polyclonal	1:250
GFP	Abcam, ab1218	Mouse Monoclonal	1:250
c-Myc	Developmental Studies Hybridoma Bank (DSHB), 9E 10	Mouse Monoclonal	1:200
c-Myc	Merck, PLA0001	Rabbit Polyclonal	1:200
6-His-Tag	Abcam, ab3554	Chicken Polyclonal, FITC	1:100
T7-Tag	Invitrogen, PA1-32390	Goat Polyclonal, FITC	1:200
***X. laevis* Marcks**	Genscript, custom-made	Rabbit Polyclonal	1:200
***X. laevis* Marcksl1**	Genscript, custom-made	Rabbit Polyclonal	1:100
Sox2	Cell Signaling Technology (CST), D6D9	Rabbit Monoclonal	1:100
Sox3	Zhang et al., 2004	Rabbit Polyclonal	1:100

1215

Supplementary figures

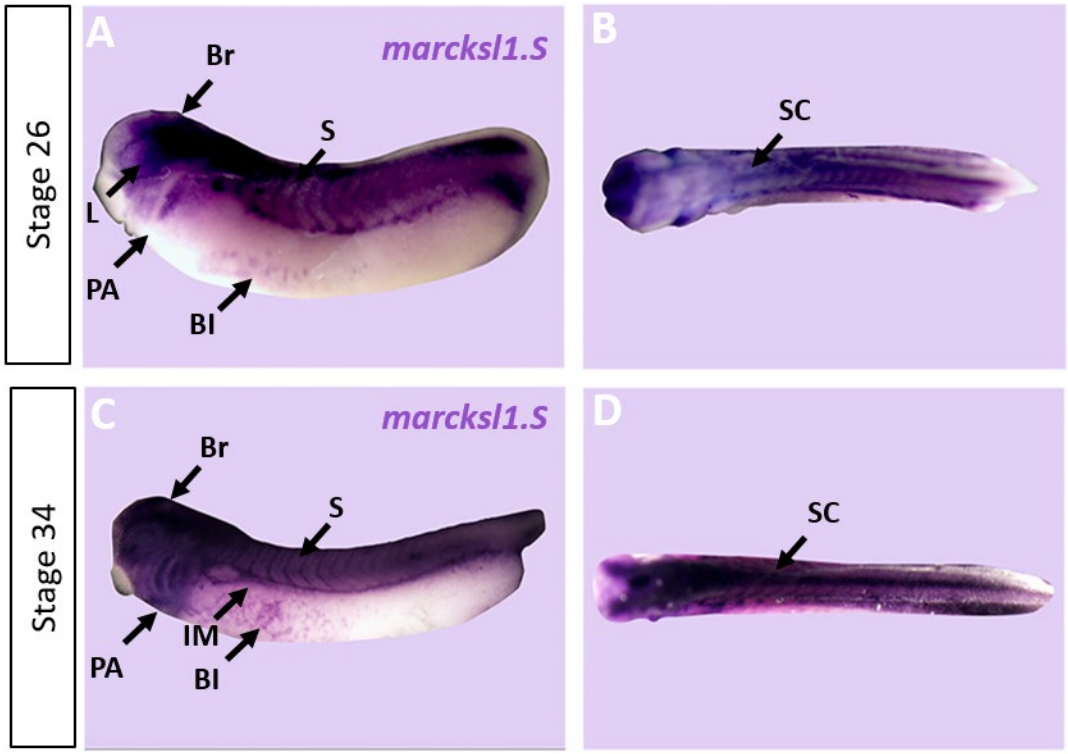

Fig. S1: Expression of *marcksl1. S* in *Xenopus.*
Expression of *marcksl1.S* as revealed by whole mount in situ hybridization in stage 26 (A-B) and 34 (C-D) *Xenopus* embryos in lateral (A,C) and dorsal (B, D) views (anterior is to the left). Expression in the brain (Br), spinal cord (SC), lens (L), somites (S), intermediate mesoderm (IM), blood islands (Bl), and pharyngeal arches (PA) is indicated.

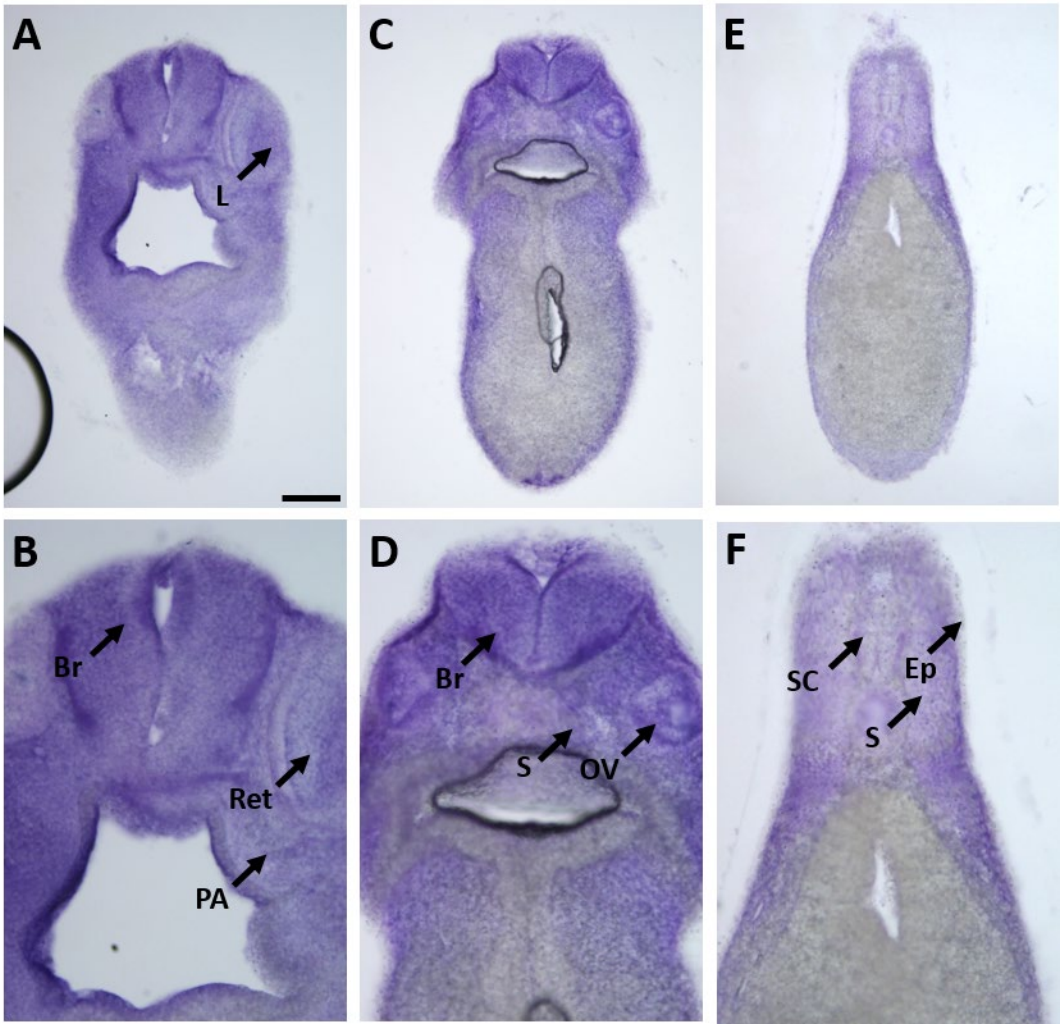

Fig. S2: Expression of *marcks.S* mRNA revealed by transverse vibratome sections of *Xenopus* stage 34 embryos after whole-mount in situ hybridization.
Higher magnification details of (A, C, E) are shown in (B, D, F), respectively. *marcks*.S expression is evident in the brain (Br), retinas (Ret), lens (L), spinal cord (SC), PA, otic vesicle (OV), epidermis (Ep), and somites (S). Scale bar in A = 100 µm for (A, C, E) and 50 µm for (B, D, F).

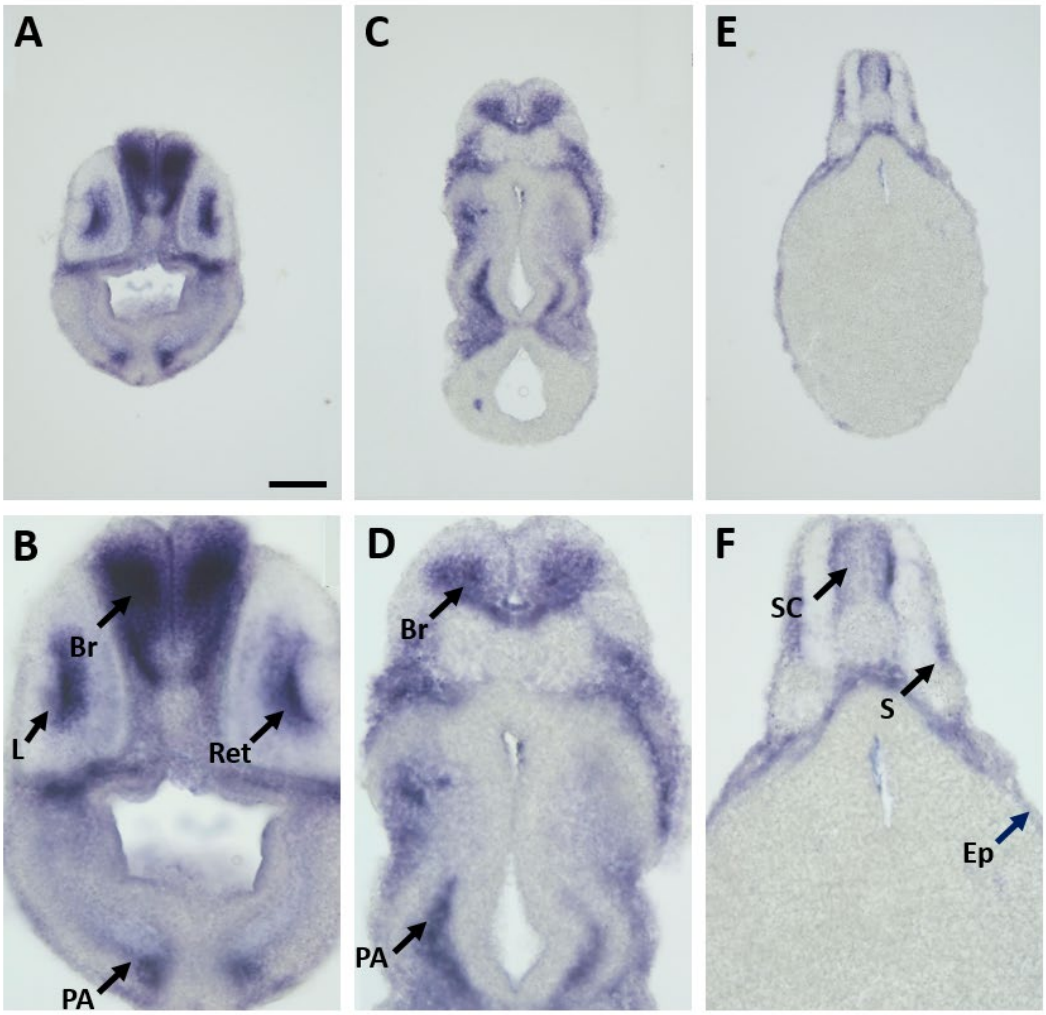

Fig. S3: Expression of *marcksl1.L* mRNA as revealed by transverse vibratome sections of *Xenopus* stage 34 embryos after whole-mount in situ hybridization.
Higher magnification details of (A, C, E) are shown in (B, D, F), respectively. *marcks*l1.L expression is evident in the brain (Br), retinas (Ret), lens (L), spinal cord (SC), PA, epidermis (Ep), and somites (S). Scale bar in A = 100 µm for (A, C, E) and 50 µm for (B, D, F).

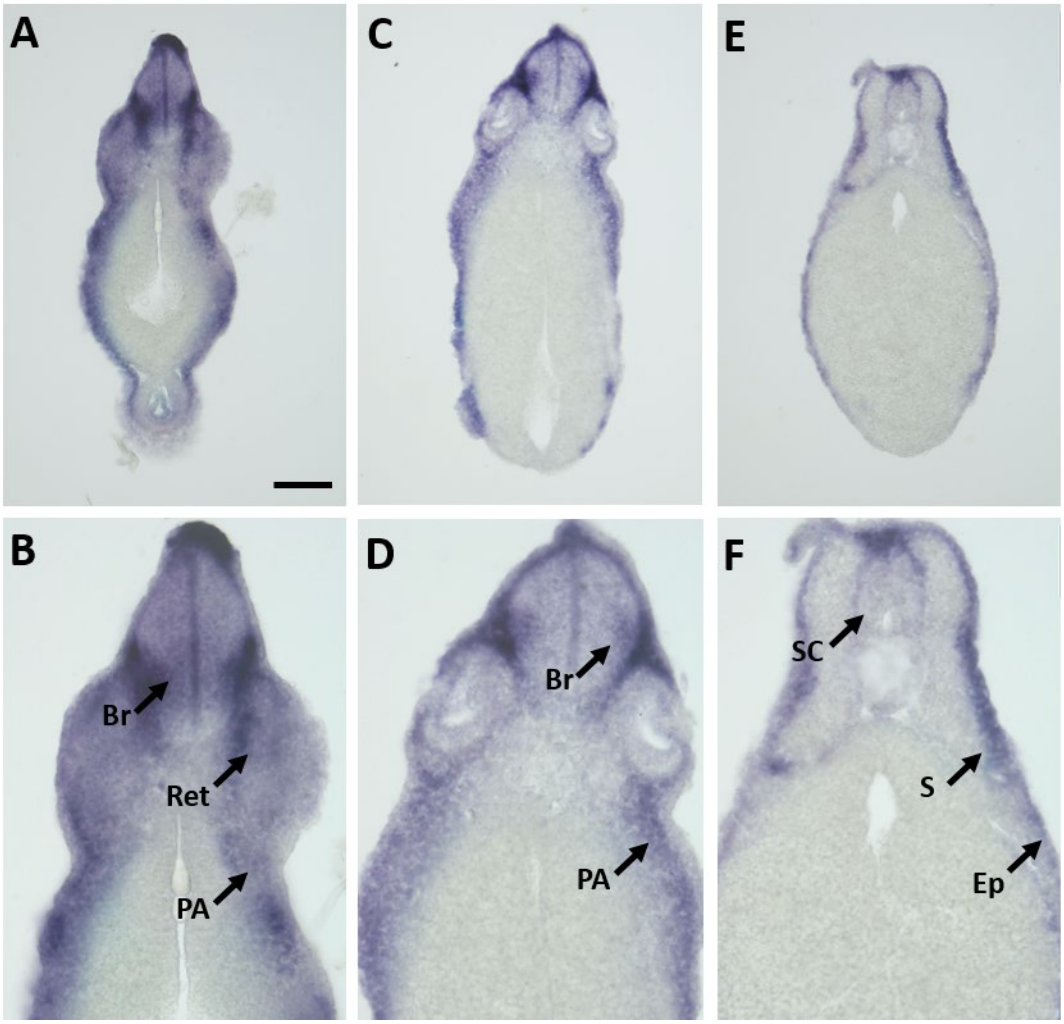

Fig. S4: Expression of *marcksl1.S* mRNA as revealed by transverse vibratome sections of *Xenopus* stage 34 embryos after whole-mount in situ hybridization.
Higher magnification details of (A, C) are shown in (B, D). *marcks*l1.L expression is evident in the brain (Br), retinas (Ret), spinal cord (SC), pharyngeal arches (PA), epidermis (Ep), and somites (S). Scale bar in A = 100 µm for (A, C) and 50 µm for (B, D).

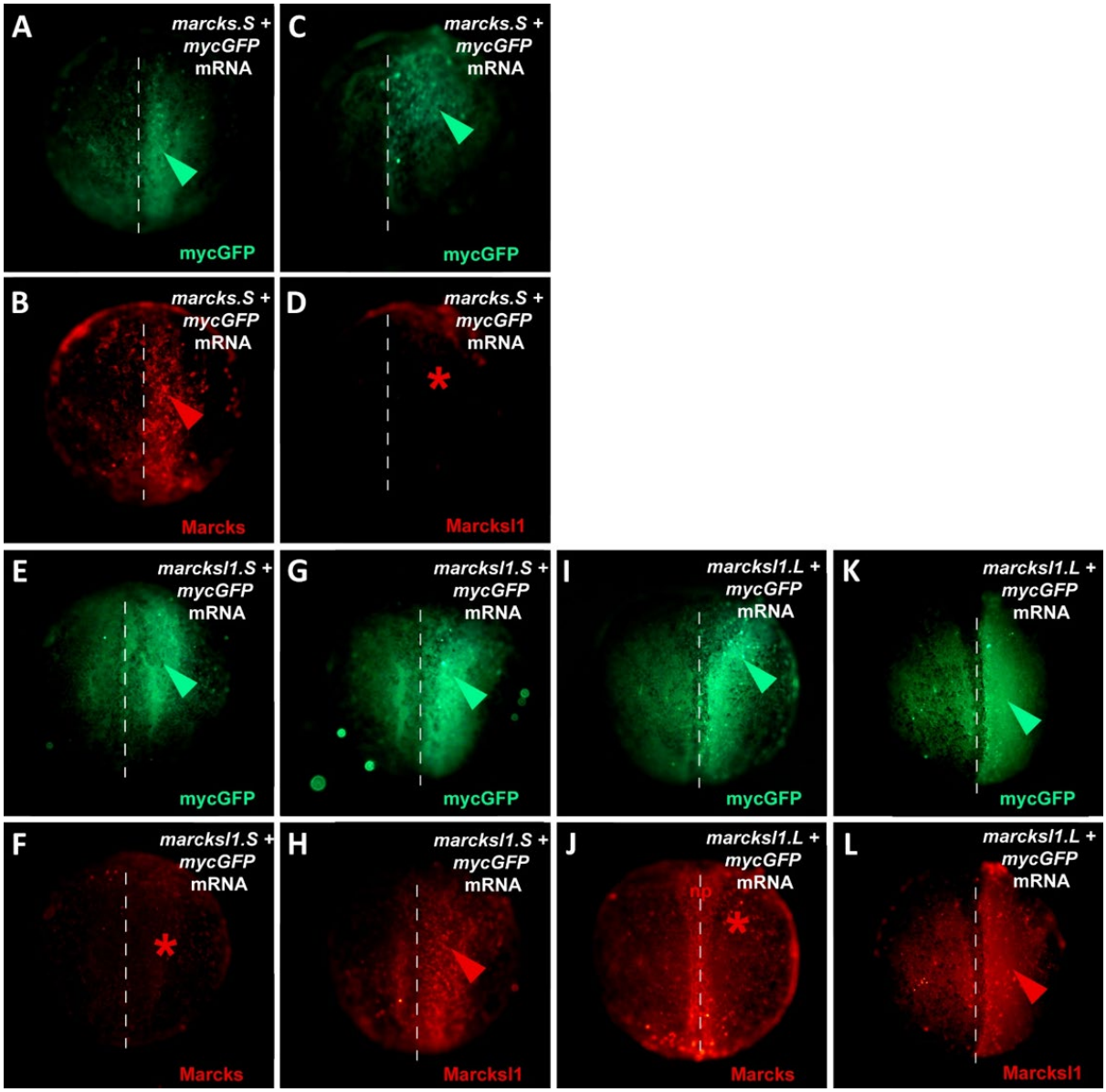

Fig. S5: Specificity of Marcks and Marcksl1 antibodies.
One blastomere of 2-cell stage embryos was co-injected with 125 pg of mycGFP mRNA and 500 pg of either *marcksS* mRNA (A-D), *marcksl1.S* mRNA (E-H), or *marcksl1.L* mRNA (I-L) followed by immunostaining at neural plate stages (stage 13-16) with anti-Myc (A, C, E, G, I, K) and either anti-Marcks (B, F, J) or anti-Marcksl1 (D, H, L) antibodies. The injected side is shown on the right, with the injected area indicated by mycGFP immunostaining (green arrowheads). Anti-Marcks antibodies recognize Marcks (B, red arrowhead) but not Marcksl1 (F, I, red asterisks) proteins, while anti-Marcksl1 antibodies recognize Marcksl1 (H, L, red arrowheads) but not Marcks (D, red asterisk) proteins translated from the injected mRNAs indicating that antibodies do not cross-react. Marcks antibodies also detected native Marcks1 protein in the neural plate in (np) in embryos at late neural plate stages (J).

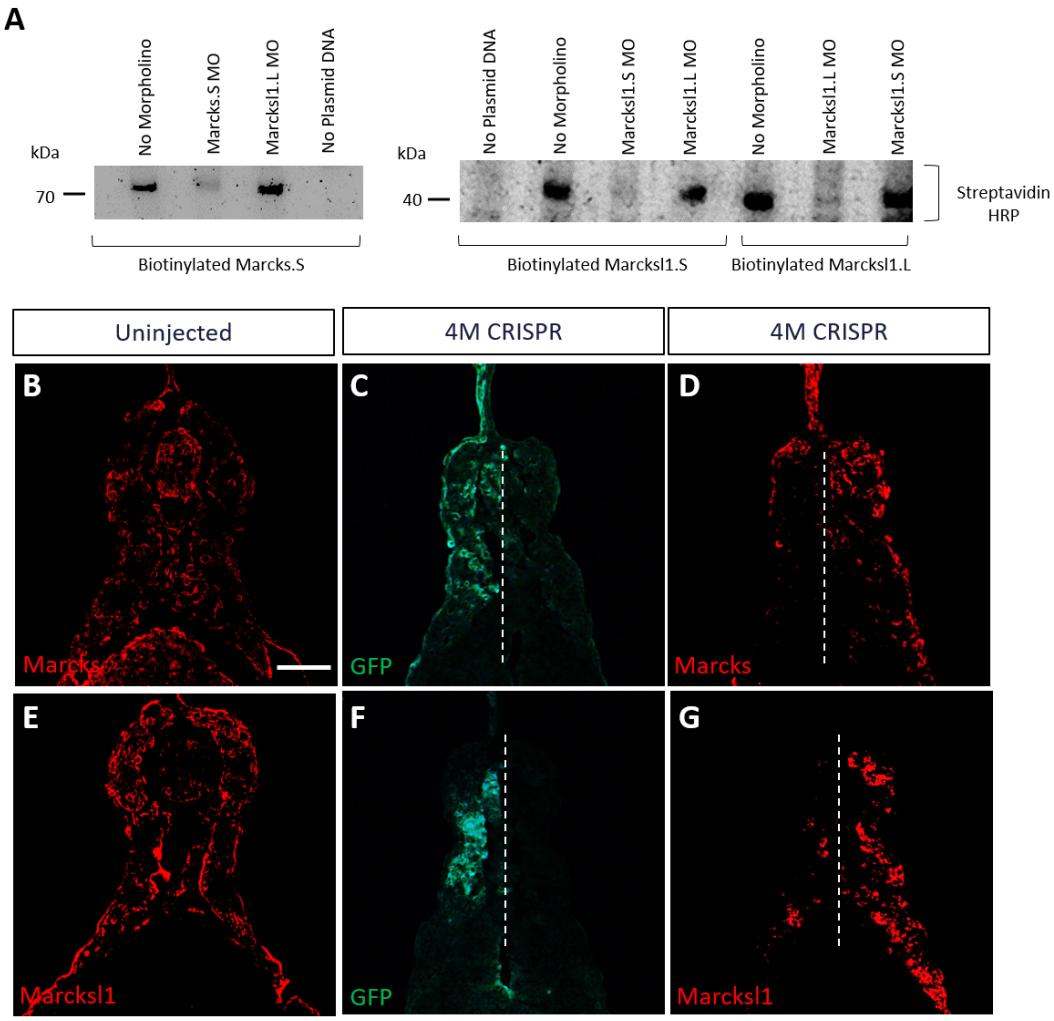

Fig. S6: Validation of Marcks and Marcksl1 knockdown and knockout.
A: Morpholino (MO) specificity and efficacy verified by in vitro TNT. Biotinylated Marcks.S, Marcksl1.L, and Marcksl1.S proteins were expressed by in vitro transcription and translation (TNT) and detected in western plots by Streptavidin-HRP. In vitro, TNT reactions without any morpholino added served as positive control. In vitro, TNT reactions without plasmid DNA added served as negative control. Protein translation was blocked when the appropriate MO was added, but not by an inappropriate MO. B-G: Reduction of Marcks and Marcksl1 immunostaining in stage 36 embryos co-injected with *marcks.L/S*, *marcksl1.L/S* sgRNA and *myc-GFP* mRNA (4M CRISPR). In uninjected embryos (B, E), Marcks (B) and Marcksl1 (E) expression are seen on both sides. In 4M CRISPR-injected embryos Marcks (D) and Marcksl1 (G) immunostaining is reduced on the injected side as indicated by GFP immunostaining (C, F). Scale bar in B = 50 µm (for all panels).

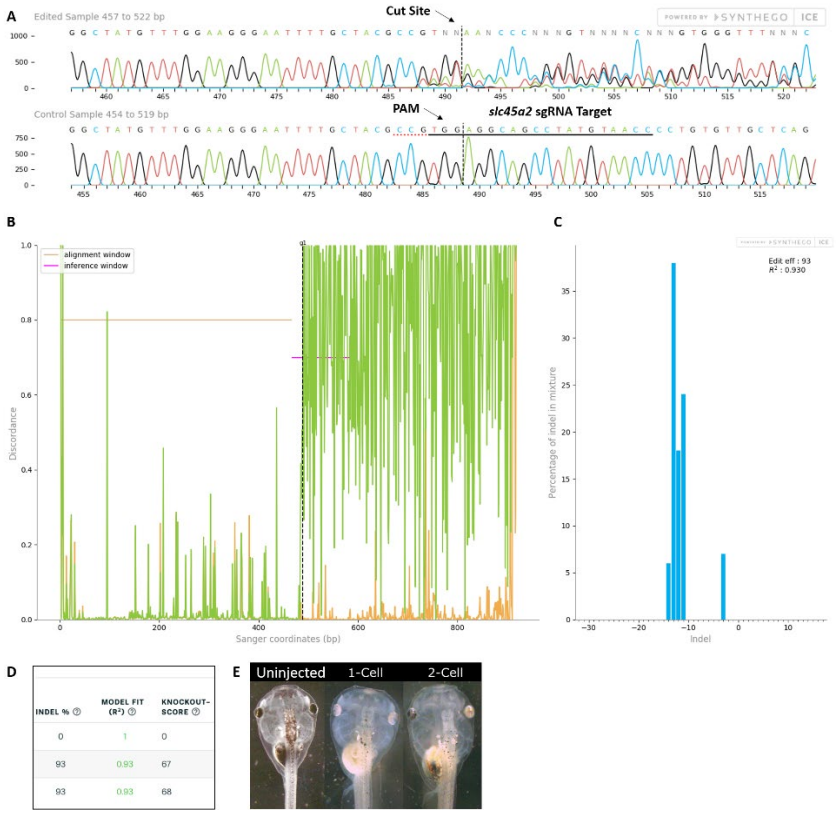

Fig. S7: Control *slc45a2* sgRNA/Cas9 efficiently and specifically edits targeted *X. laevis* DNA.

All data were generated by the Synthego Inference for CRISPR Edits (ICE) tool based on DNA samples from stage 26-42 embryos injected with *slc45a2* sgRNA, Cas9 protein, and *myc-GFP* mRNA during the 1-cell stage in comparison with uninjected embryos. A: Sanger sequence chromatograms showing degradation of the sequence trace from PCR products amplifying CRISPR-targeted *slc45a2* DNA (top) compared with DNA from uninjected embryos (bottom). The underlined region indicates the sgRNA target binding sequence. Arrows indicate the Protospacer Adjacent Motif (PAM) and the Cas9 cleavage site. B: Discordance plot showing the level of sequence-base disagreement between the control reference DNA from uninjected embryos (orange lines) and the CRISPR DNA (green lines) in the region surrounding the cut site, indicating a high level of sequence difference after the cleavage site, shown by the hatched line. C: Synthego Indel Distribution plot, which infers the distribution of insertion-deletion sizes (± 1 or more nucleotides) around the *slc45a2* CRISPR-target site. The x-axis indicates the size of the indel, and the y-axis shows the percentage of the sequences containing it. The editing efficiency score indicates that 93% of the DNA in the CRISPR-targeted sequence was edited. A Pearson correlation coefficient (R^2) was also generated by ICE with a value of 0.93 out of 1, measuring how well the indel distribution fits the Sanger sequence data. D: Summary of three analyzed samples showing the sgRNA target and PAM sequences. DNA from PCR products comparing two *slc45a2* sequences from uninjected embryos (top) shows an indel percentage of 0% and a predicted knockout (KO) score of 0%. Indel scores for DNA sequences derived from two CRISPR-edited embryos (middle and bottom) indicate that 93% of the DNA analyzed was edited. Knockout scores of 67-68% indicate the proportion of indels that contain a frameshift mutation or a 21+ base-pair indel. E: *slc45a2* CRISPR knockout generates a visible loss of eye pigmentation in stage 46 tadpoles. Whereas uninjected tadpoles have no eye pigmentation defects, eye pigmentation is unilaterally reduced in the CRISPR-injected side of 2-cell stage-injected embryos and bilaterally reduced in 1-cell stage CRISPR-injected embryos.

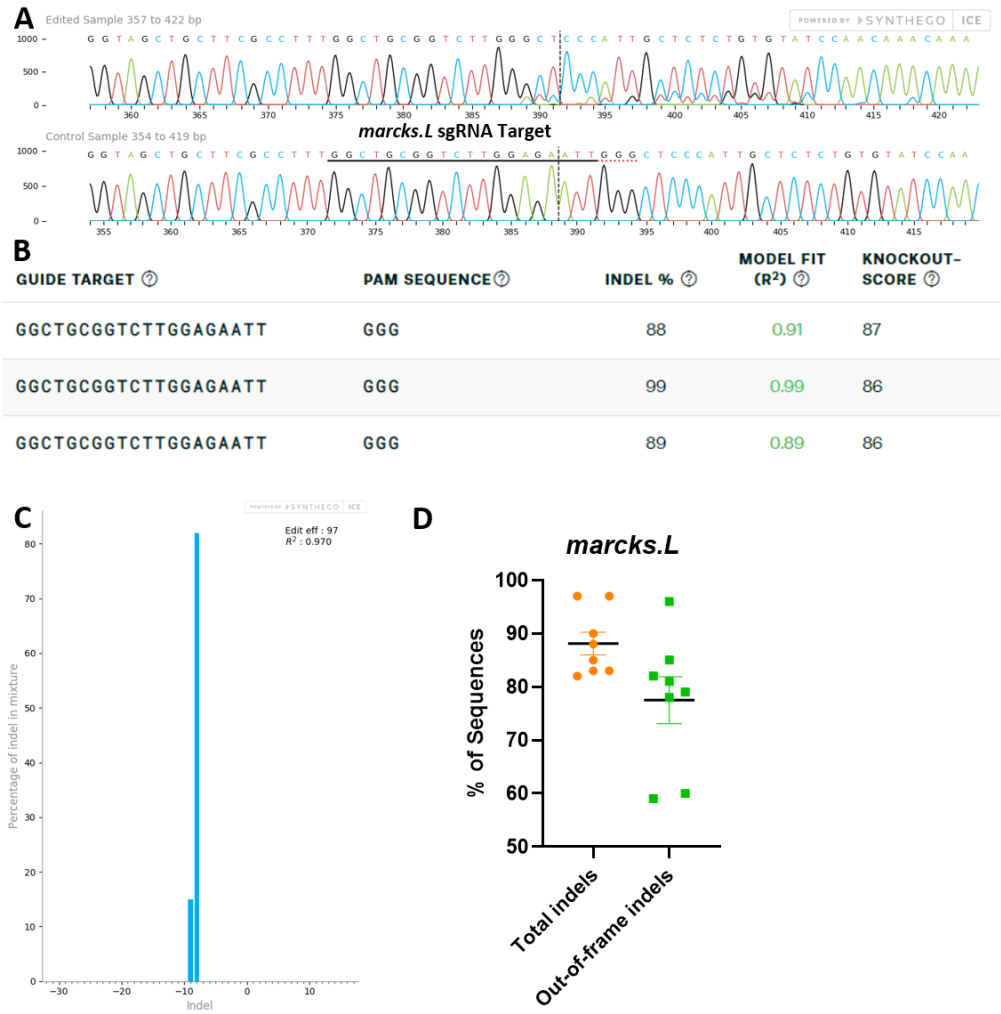

Fig. S8: *marcks.L/S* sgRNA efficiently and specifically edits *Xenopus laevis marcks.L* DNA.

All data were generated by the Synthego Inference for CRISPR Edits (ICE) tool based on DNA samples from stage 26-42 embryos injected with *marcks.L/S and marcksl1.L/S* sgRNA, Cas9 protein, and *myc-GFP* mRNA during the 1-cell stage in comparison with uninjected embryos. A: Sanger sequence chromatograms showing degradation of the sequence trace from PCR products amplifying CRISPR-targeted *marcks.L* exon 1 DNA (top) compared with DNA from an uninjected embryo (bottom). The underlined region indicates the sgRNA target binding sequence. B: Summary of three analyzed samples showing the sgRNA target and PAM sequence. Indel scores for DNA sequences derived from 3 CRISPR-edited embryos compared with uninjected embryos, indicating that 88%, 89%, and 99% of the DNA analyzed was edited. Knockout scores of 86% and 87% indicate the proportion of indels that contain a frameshift mutation. C: Synthego Indel Distribution plot from one representative CRISPR-embryo, which infers the distribution of insertion-deletion sizes (± 1 or more nucleotides) around the *marcks.L* CRISPR-target site. The x-axis indicates the size of the indel, and the y-axis shows the percentage of the sequences containing it. The editing efficiency score indicates that 97% of the DNA in the CRISPR-targeted sequence was edited with mostly an eight-base-pair deletion. A Pearson correlation coefficient (R^2) was also generated by ICE with a value of 0.97 out of 1, measuring how well the indel distribution fits the Sanger sequence data. D: Indel percentages calculated by ICE for 8 CRISPR-edited embryos, indicating that an average of 88% of the DNA was edited for all animals. From this edited DNA, 78% contained out-of-frame mutations.

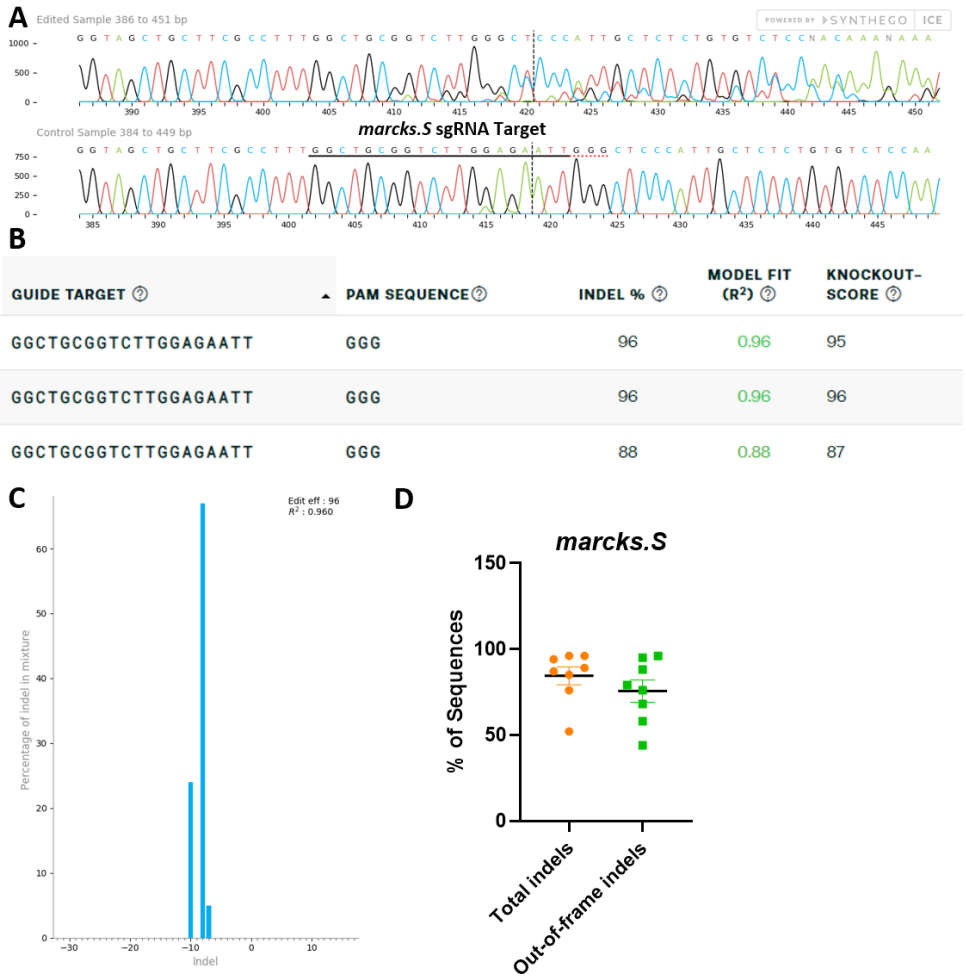

Fig. S9: *marcks.L/S* sgRNA efficiently and specifically edits *Xenopus laevis marcks.S* DNA. All data were generated by the Synthego ICE tool based on DNA samples from stage 26-42 embryos injected with *marcks.L/S and marcksl1.L/S* sgRNA, Cas9 protein, and *myc-GFP* mRNA during the 1-cell stage in comparison with uninjected embryos. A: Sanger sequence chromatograms showing degradation of the sequence trace from PCR products amplifying CRISPR-targeted *marcks.S* exon 1 DNA (top) compared with DNA from an uninjected embryo (bottom). The underlined region indicates the sgRNA target binding sequence. B: Summary of three analyzed samples showing the sgRNA target and PAM sequence. Indel scores for DNA sequences derived from 3 CRISPR-edited embryos compared with uninjected embryos, indicating that 88% and 96% of the analyzed DNA was edited. Knockout scores of 95%, 96%, and 87% indicate the proportion of indels that contain a frameshift mutation. C: Synthego Indel Distribution plot from one representative CRISPR-embryo, which infers the distribution of insertion-deletion sizes (± 1 or more nucleotides) around the *marcks.S* CRISPR-target site. The x-axis indicates the size of the indel, and the y-axis shows the percentage of the sequences containing it. The editing efficiency score indicates that 96% of the DNA in the CRISPR-targeted sequence was edited with a majority of eight base-pair deletions. A Pearson correlation coefficient (R^2) was also generated by ICE with a value of 0.96 out of 1, measuring how well the indel distribution fits the Sanger sequence data. D: Indel percentages calculated by ICE for 8 CRISPR-edited embryos, indicating that an average of 84% of the DNA was edited for all animals. From this edited DNA, 76% contained out-of-frame mutations.

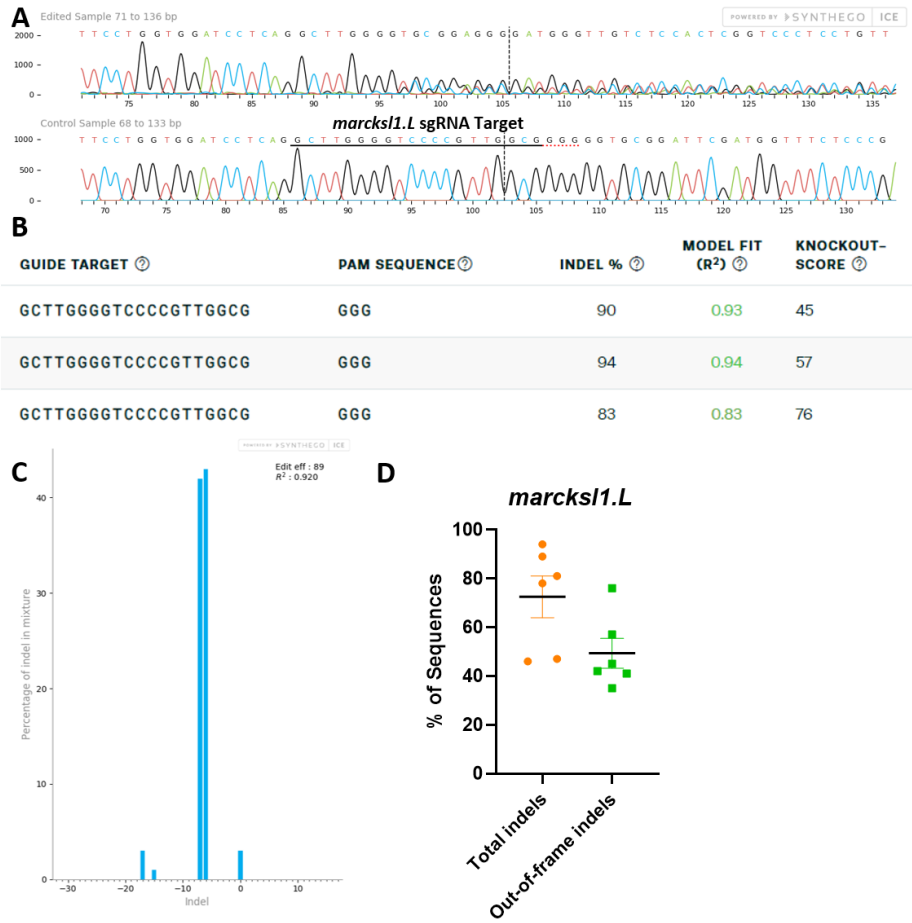

Fig. S10: *marcksl1.L/S* sgRNA efficiently and specifically edits *X. laevis marcksl1.L* DNA.

All data were generated by the Synthego Inference for CRISPR Edits (ICE) tool based on DNA samples from stage 26-42 embryos injected with *marcks.L/S and marcksl1.L/S* sgRNA, Cas9 protein, and *myc-GFP* mRNA during the 1-cell stage in comparison with uninjected embryos. A: Sanger sequence chromatograms showing degradation of the sequence trace from PCR products amplifying CRISPR-targeted *marcksl1.L* exon 2 DNA (top) compared with DNA from an uninjected embryo (bottom). The underlined region indicates the sgRNA target binding sequence. B: Summary of three analyzed samples showing the sgRNA target and PAM sequence. Indel scores for DNA sequences derived from 3 CRISPR-edited embryos compared with uninjected embryos, indicating that 83%, 90%, and 94% of the DNA analyzed was edited. Knockout scores of 45%, 57%, and 76% indicate the proportion of indels that contain a frameshift mutation. C: Synthego Indel Distribution plot from one representative CRISPR-embryo, which infers the distribution of insertion-deletion sizes (± 1 or more nucleotides) around the *marcksl1.L* CRISPR-target site. The x-axis indicates the size of the indel, and the y-axis shows the percentage of the sequences containing it. The editing efficiency score indicates that 89% of the DNA in the CRISPR-targeted sequence was edited with mostly 6-7 base-pair deletions. A Pearson correlation coefficient (R^2) was also generated by ICE with a value of 0.92 out of 1, measuring how well the indel distribution fits the Sanger sequence data. D: Indel percentages calculated by ICE for 6 CRISPR-edited embryos, indicating that an average of 73% of the DNA was edited for all animals. From this edited DNA, 50% contained out-of-frame mutations.

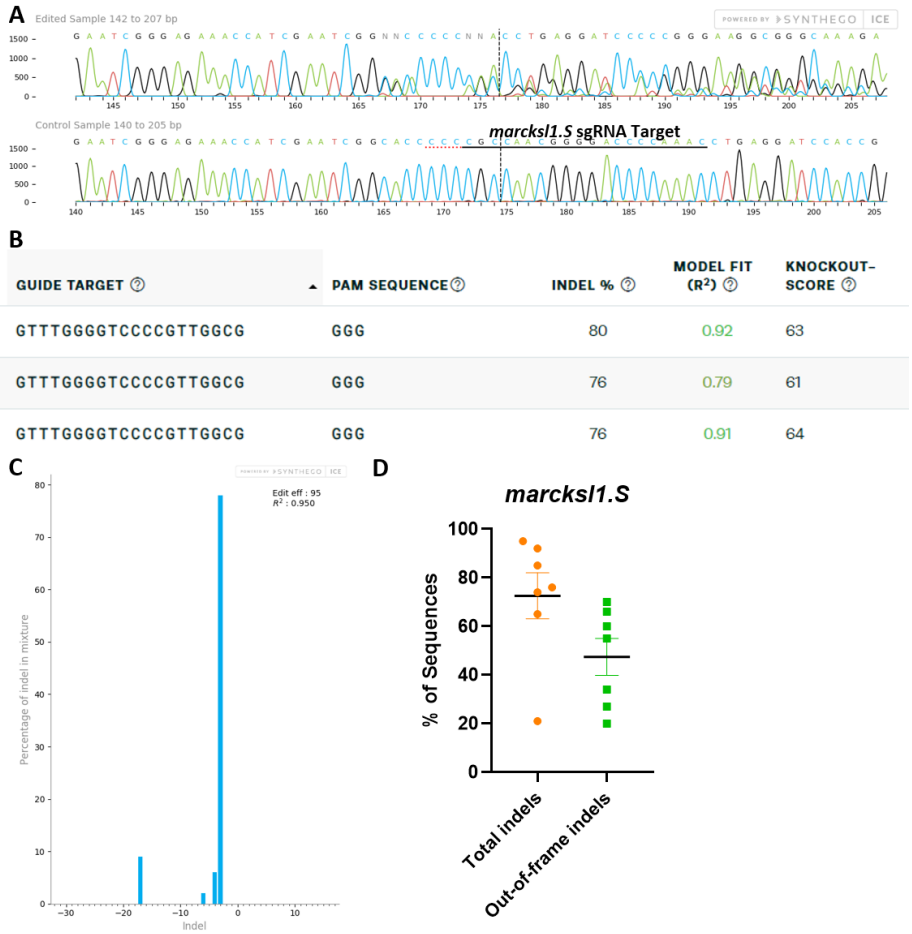

Fig. S11: *marcksl1.L/S* sgRNA efficiently and specifically edits *X. laevis marcksl1.S* DNA.

All data were generated by the Synthego Inference for CRISPR Edits (ICE) tool based on DNA samples from stage 26-42 embryos injected with *marcks.L/S and marcksl1.L/S* sgRNA, Cas9 protein, and *myc-GFP* mRNA during the 1-cell stage in comparison with uninjected embryos. A: Sanger sequence chromatograms showing degradation of the sequence trace from PCR products amplifying CRISPR-targeted *marcksl1.S* exon 2 DNA (top) compared with DNA from an uninjected embryo (bottom). The underlined region indicates the sgRNA target binding sequence. B: Summary of three analyzed samples showing the sgRNA target and PAM sequence. Indel scores for DNA sequences derived from 3 CRISPR-edited embryos compared with uninjected embryos, indicating that 76% and 80% of the DNA analyzed was edited. Knockout scores of 61%, 63%, and 64% indicate the proportion of indels that contain a frameshift mutation. C: Synthego Indel Distribution plot from one representative CRISPR-embryo, which infers the distribution of insertion-deletion sizes (± 1 or more nucleotides) around the *marcksl1.S* CRISPR-target site. The x-axis indicates the size of the indel, and the y-axis shows the percentage of the sequences containing it. The editing efficiency score indicates that 95% of the DNA in the CRISPR-targeted sequence was edited with mostly a 3-base-pair deletion. A Pearson correlation coefficient (R^2) was also generated by ICE with a value of 0.95 out of 1, measuring how well the indel distribution fits the Sanger sequence data. D: Indel percentages calculated by ICE for 7 CRISPR-edited embryos, indicating that an average of 73% of the DNA was edited for all animals. From this edited DNA, 47% contained out-of-frame mutations.

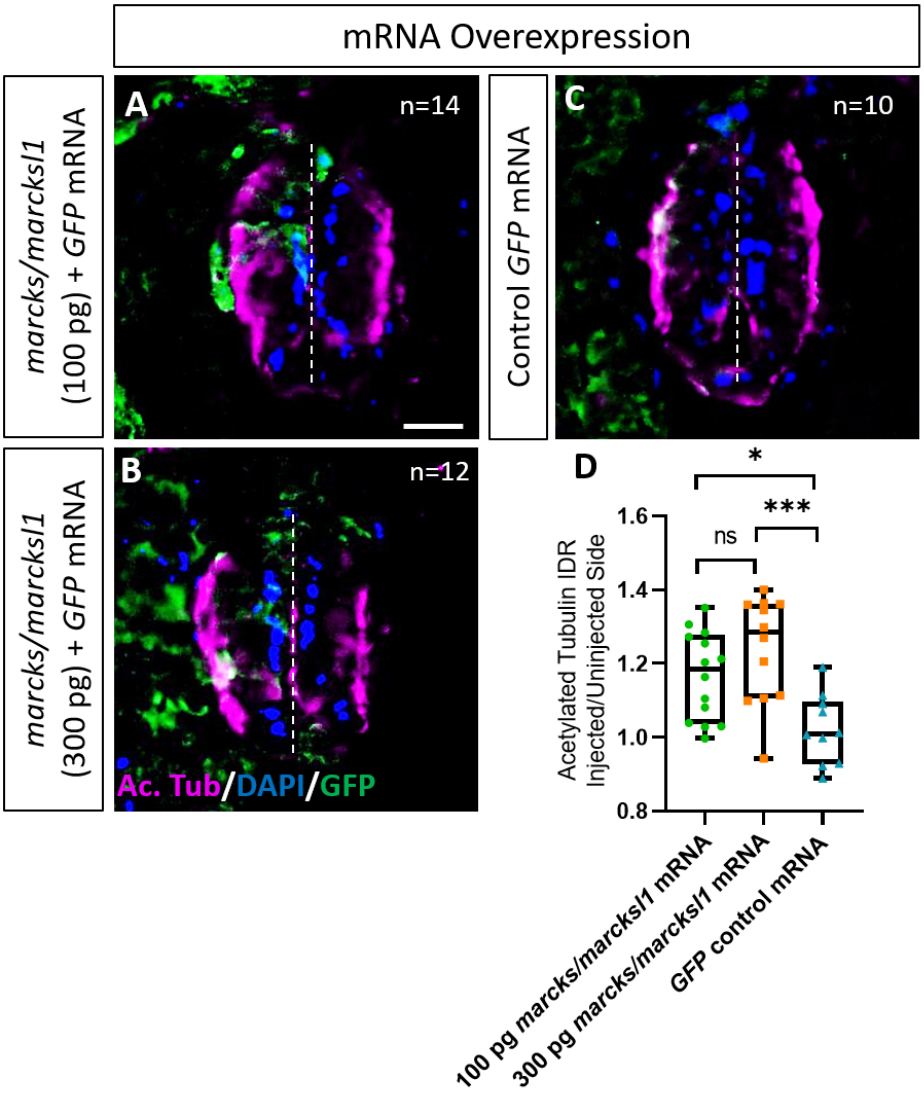

Fig. S12: Marcks and Marcksl1 overexpression promotes neurite outgrowth during *Xenopus* spinal cord development.
One blastomere of 4-8 cell stage embryos was co-injected with 100 pg (A) and 300 pg (B) of each *marcks*.S, *marcksl1.L,* and *marcksl1.S* mRNA in addition to 125 pg *myc-GFP* mRNA. In control embryos, 125 pg *myc-GFP* mRNA was injected (C). Injected (left) and uninjected (right) spinal cord sides of stage 34-36 embryos (separated by the dashed line) were compared in transverse sections immunostained for acetylated tubulin (A-C) and for GFP to determine the injected side. Compared to control embryos, immunostaining for acetylated tubulin was quantified (D) by determining the integrated density ratio (IDR) of staining in injected to uninjected sides. Significance was determined using an ordinary one-way ANOVA with Tukey's multiple comparisons test. NS, not significant; *P<0.05; ***P<0.001. Error bars represent minimum to maximum values showing all points with the line at mean. n refers to the number of animals analyzed. Scale bar in A = 25 µm (for all panels).

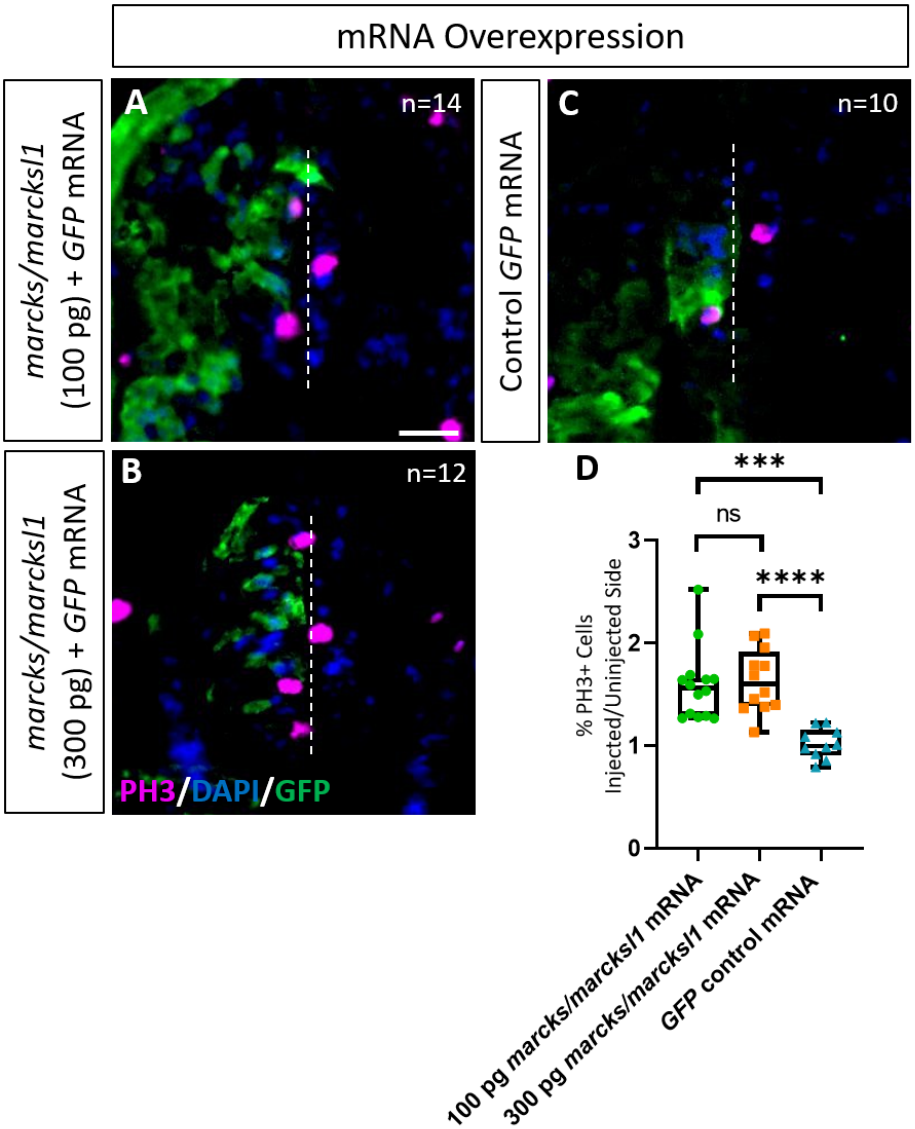

Fig. S13: Marcks and Marcksl1 overexpression promotes mitotic activity during *Xenopus* spinal cord development.
One blastomere of 4-8 cell stage embryos was co-injected with 100 pg (A) and 300 pg (B) of each *marcks*.S, marcksl1.*L,* and *marcksl1.S* mRNA in addition to 125 pg *myc-GFP* mRNA. In control embryos, 125 pg *myc-GFP* mRNA was injected (C). Injected (left) and uninjected (right) spinal cord sides of stage 34-36 embryos (separated by the dashed line) were compared in transverse sections immunostained for PH3 (A-C) and for GFP to determine the injected side. Immunostaining for acetylated tubulin was quantified (D) by determining the ratio of the percentage of PH3+ cells in injected and uninjected sides in comparison with control embryos. Significance was determined using an ordinary one-way ANOVA with Tukey's multiple comparisons test. NS, not significant; ***P<0.001. Error bars represent minimum to maximum values showing all points with the line at the mean. n refers to the number of animals analyzed. Scale bar in A = 25 µm (for all panels).

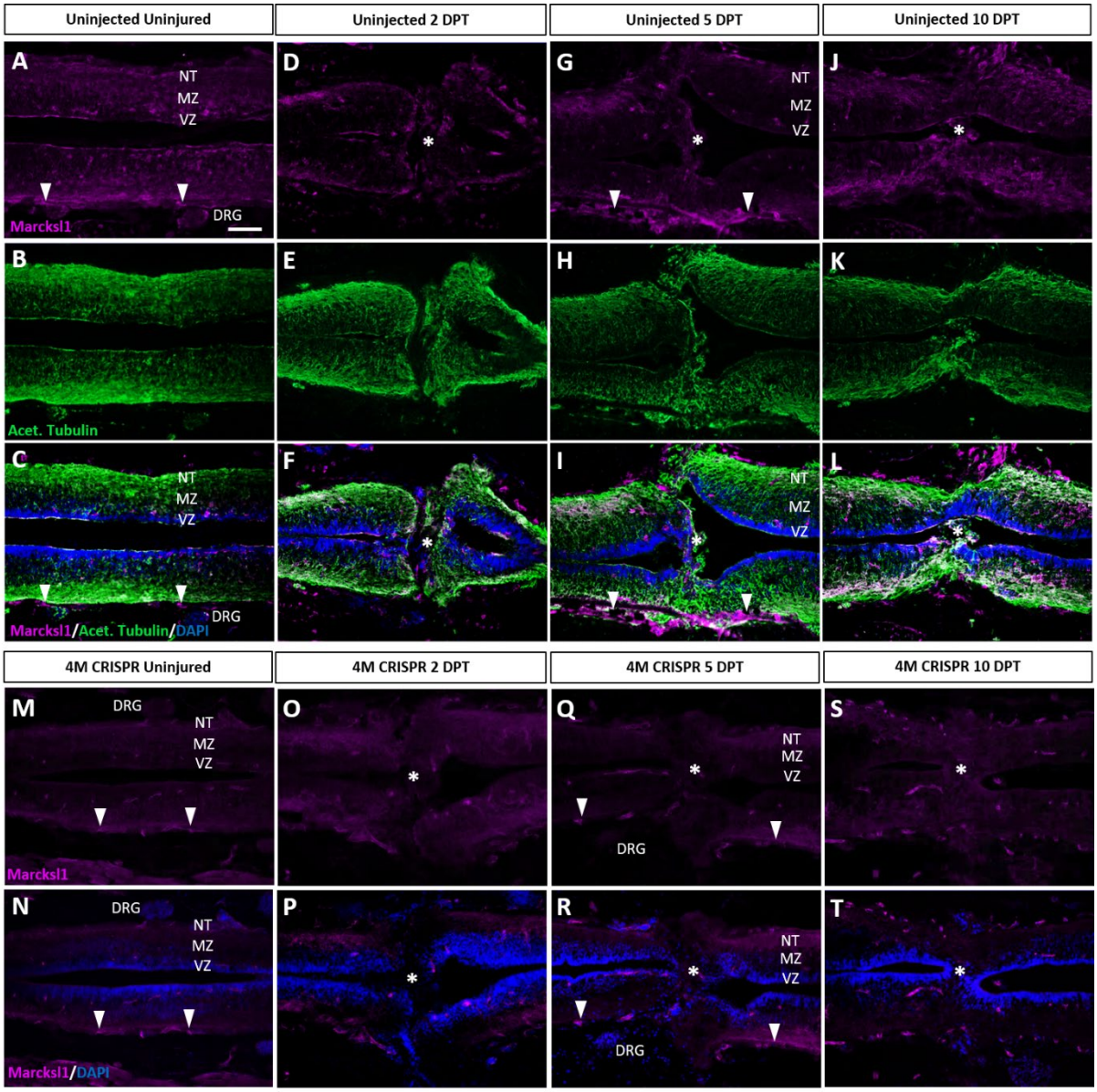

Fig. S14 Marcksl1 proteins are upregulated after spinal cord transection in uninjected but not in 4M CRISPR-injected tadpoles.

A-L: Immunostaining for Marcksl1 in horizontal sections of uninjected stage 50 tadpoles without injury (A-C) or at 2 DPT (D-F), 5 DPT (G-I), and 10 DPT (J-L). Before the injury, Marcksl1 immunostaining was weakly detected in the ventricular zone (VZ), mantle zone (MZ) and the neurite tracts (NT) of the marginal zone of the spinal as well as in the meninges (white arrowheads) and dorsal root ganglia (DRG). After spinal cord transection, it was slightly upregulated in cells infiltrating the injury site (white asterisks) and in all layers of the spinal cord surrounding the injury gap at 10 DPT. N=6 tadpoles per condition. M-T: Immunostaining for Marcksl1 in horizontal sections of 4M CRISPR-injected stage 50 tadpoles without injury (M, N) or at 2 DPT (O, P), 5 DPT (Q, R), and 10 DPT (S, T). Barely any Marcksl1 immunostaining is detectable at any time point. N=6 tadpoles per condition. Scale bar in A = 50 µm (for all panels).

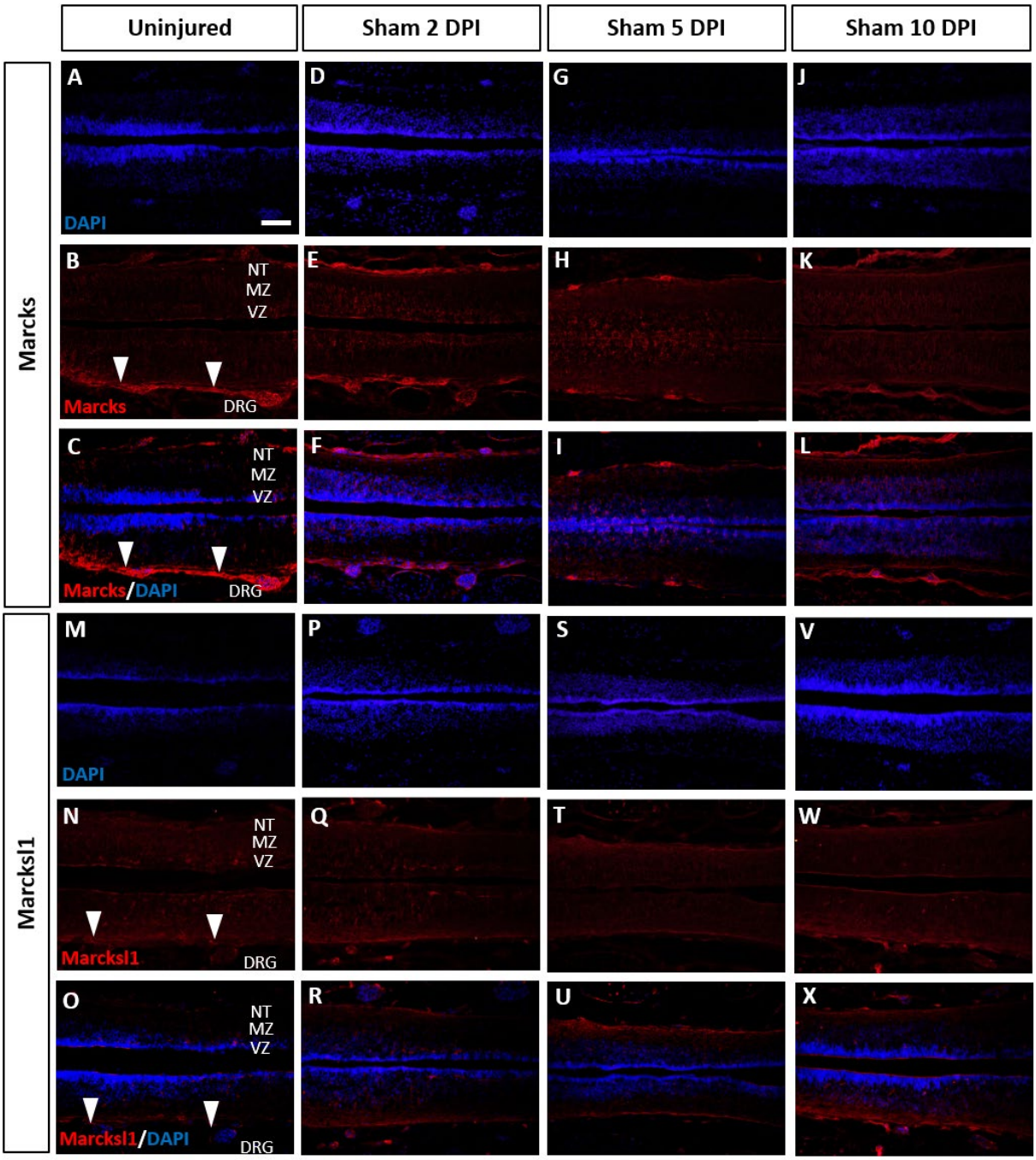

Fig. S15: Marcks and Marcksl1 proteins do not change in uninjected sham-operated tadpoles.
Immunostaining for Marcks (A-L) and Marcksl1 (M-X) in sham-operated tadpoles remained unaltered compared to the uninjured condition (A-C, M-O) at two days (D-F, P-R), five days (G-I, S-U), and ten days (J-L, V-X) post-injury (DPI). N= 3 tadpoles per condition. White arrowheads indicate the meninges. Abbreviations: DRG: dorsal root ganglia; MZ: mantle zone; NT of the marginal zone; VZ: ventricular zone. Scale bar in A= 50 µm (for all panels).

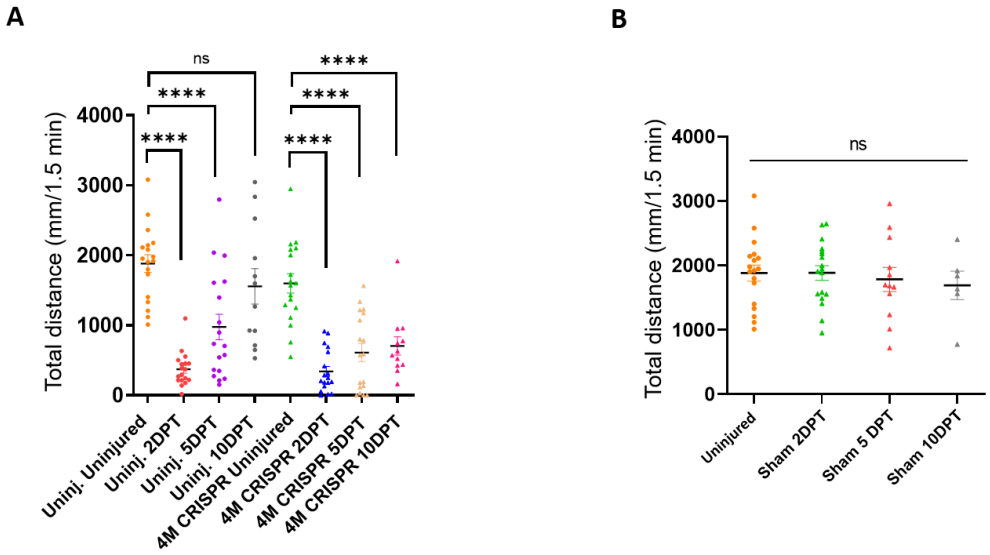

Fig. S16: Functional recovery after spinal cord transection is compromised after knockout of Marcks and Marcksl1.

A: Swimming recovery test in stage 50 wild-type and CRISPR tadpoles after spinal cord injury. The graph shows the total swimming distance in uninjected and 4M CRISPR-injected animals before the injury and at 2-, 5-, and 10- DPT. The y-axis indicates the distance traveled by the tadpoles in millimeters for 90 seconds (same data as in Fig. 6A but different statistical comparison). Significance was determined using an ordinary one-way ANOVA with uncorrected Fisher's LSD for multiple comparisons. NS, not significant; ***P<0.001. All data points are shown with the line at mean. Error bars represent SEM. B: Swimming test in stage 50 sham-operated tadpoles reveals no effect on swimming performance. The graph shows the total swimming distance before the injury and 2-, 5-, and 10-days post-sham-injury (DPI). Significance was determined using an ordinary one-way ANOVA with uncorrected Fisher's LSD for multiple comparisons. NS is not significant. All data points are shown with the line at mean. Error bars represent SEM.

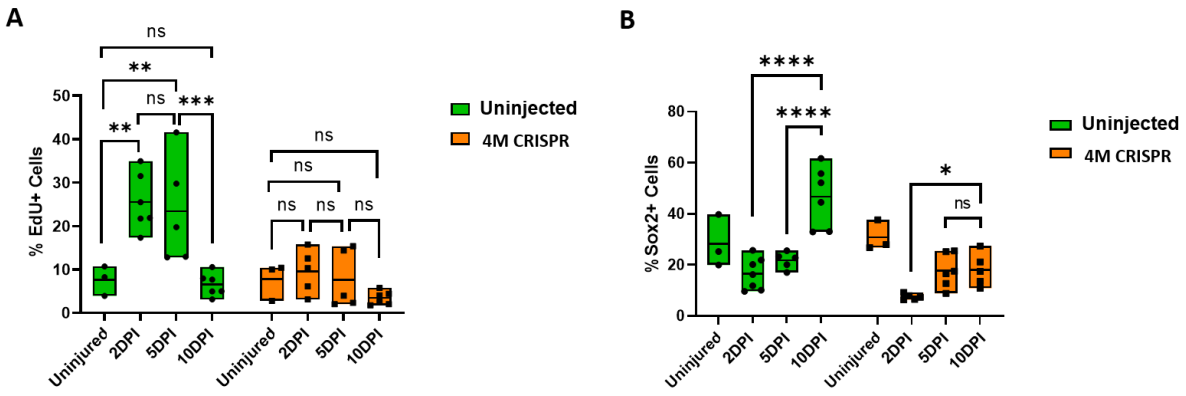

Fig. S17: Upregulation of cell proliferation and Sox2+ neuro-glial progenitors after spinal cord transection is compromised after the knockout of Marcks and Marcksl1.
A: Quantification of EdU+ cells at 2-, 5-, and 10-DPI in sham-operated tadpoles at stage 50 (same data as in Fig. 7 I but different statistical comparison). B: Quantification of Sox2+ cells at 2-, 5-, and 10-days post transection (DPI) in sham-operated tadpoles at stage 50 (same data as in Fig. 8 I but different statistical comparison). Significance was determined using a 2-way ANOVA with Sidak's multiple comparisons test. NS, not significant; *P<0.05; **P≤0.01; ***P<0.001; ****P<0.0001. All data points are shown with the line at mean.

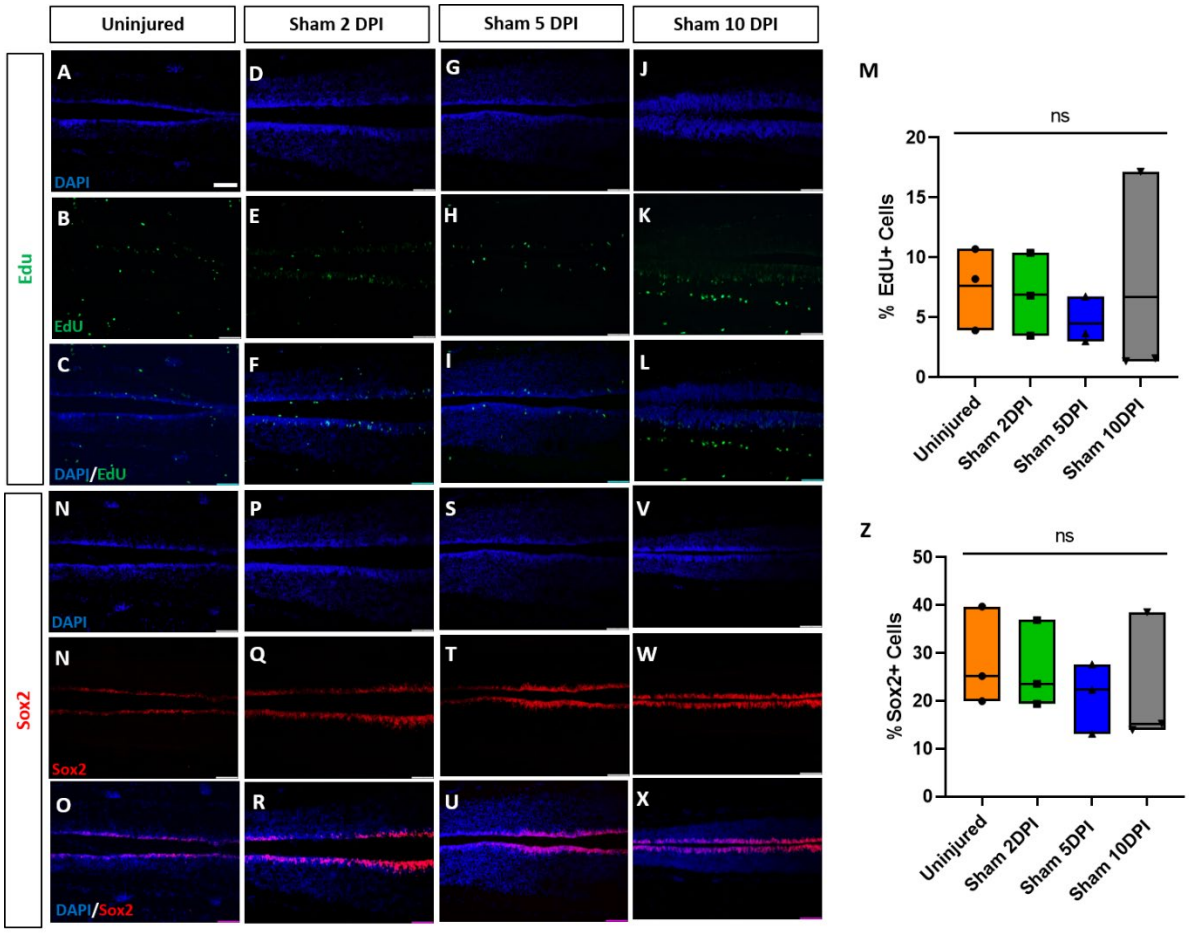

Fig. S18: Sham-operated animals show no alterations of proliferation or numbers of neuro-glial progenitors.

Evaluation and quantification of EdU+ proliferative cells (A-M) and Sox2+ neuro-glial progenitors (N-Z) at 2-, 5-, and 10-DPI in horizontal sections of sham-operated tadpoles at stage 50. Significance was determined using a 2-way ANOVA with Sidak's multiple comparisons test. NS, not significant; *P<0.05; **P≤0.01; ***P<0.001; ****P<0.0001. All data points are shown with the line at mean. Scale bar in A= 50 µm (for all panels).